SEPTEMBER 1957 VOLUME 1 (1957) No. 5

GREGG M. SINCLAIR LIBRARY
UNIVERSITY OF HAWAII
8-6-63

NUCLEAR INSTRUMENTS

A JOURNAL ON ACCELERATORS, INSTRUMENTATION AND TECHNIQUES IN NUCLEAR PHYSICS

EDITOR K. SIEGBAHN – UPPSALA

CONTENTS

Editor's Note. 233

S. BERGLUND, R. NILSSON, P. OHLIN, K. SIEGBAHN, T. SUNDSTRÖM and S. SVENNERSTEDT, Fusion experiments in deuterium plasma. 233

R. J. WALEN, Transformation d'une focalisation de premier ordre en focalisation de deuxième ordre en spectrographie magnétique a champ homogène 242

K. G. MALMFORS, On the possibility of applying trochoidal orbits in beta-spectroscopy . . . 251

G. BÄCKSTRÖM, A device for the precision measurement of an inhomogenous magnetic field 253

A. C. VAN DORSTEN and J. H. SPAA, A high output D-D neutron generator for biological research 259

H. SCHNEIDER, An A.G. channel with four quadrupole magnets 268

B. JOHANSSON, Coincidence arrangement with high time resolution used together with a 100-channel pulse-height analyzer 274

Y. P. VARSHNI, A new particle accelerator 280

J. F. VERVIER et P. C. MACQ, Réduction des dispersions dans les détecteurs à scintillation . . 282

NORTH-HOLLAND PUBLISHING COMPANY – AMSTERDAM

NUCLEAR INSTRUMENTS

A journal on accelerators, instrumentation and techniques in nuclear physics

EDITOR: K. SIEGBAHN, UPPSALA

EDITORIAL BOARD:

J. B. ADAMS (CERN)
E. AMALDI (Rome)
H. L. ANDERSON (Chicago)
K. T. BAINBRIDGE (Cambridge, Mass.)
C. J. BAKKER (CERN)
P. R. BELL (Oak Ridge)
R. E. BELL (Montreal)
A. BERTHELOT (Saclay)
H. BRINKMAN (Groningen)
S. DE BENEDETTI (Pittsburgh)
M. DE HEMPTINNE (Louvain)
A. DE-SHALIT (Rehovoth)
M. DEUTSCH (Cambridge, Mass.)
S. DU TOIT (Pretoria)
B. S. DŽELEPOV (Leningrad)
W. GENTNER (CERN)
P. C. GUGELOT (Amsterdam)
H. HALBAN (Paris)
O. HAXEL (Heidelberg)
P. HUBER (Basel)
D. J. HUGHES (Brookhaven)
S. KIKUCHI (Tokyo)
J. KOCH (Copenhagen)
M. S. KOZODAEV (Moscow)
S. LIVINGSTON (Cambridge, Mass.)
E. M. MCMILLAN (Berkeley)
M. G. MEŠČERJAKOV (Moscow)
P. B. MOON (Birmingham)
M. L. OLIPHANT (Canberra)
W. PAUL (Bonn)
A. S. RAO (Bombay)
G. SALVINI (Rome)
P. SAVIĆ (Belgrade)
P. SCHERRER (Zürich)
CH. SCHMELZER (CERN)
H. W. B. SKINNER (Liverpool)
R. TANGEN (Blindern)
V. I. VEKSLER (Moscow)
O. WERNHOLM (Stockholm)
D. TAYLOR (Harwell)
G. VON DARDEL (CERN)
R. R. WILSON (Cornell)
S. D. WINTER (Saclay)

Contributions may be sent to the Editor, Professor K. Siegbahn, Institute of Physics, the University of Uppsala, either directly or through the intermediary of one of the members of the Editorial Board of the country or region in which the author is working. Contributions may be written in English, French or German, with an abstract in English.

Books for review should be sent to Professor Siegbahn.

Nuclear Instruments is published in bi-monthly issues. The subscription price of a volume of 360 pages is $ 17.00 (130 s), postage free.

Subscriptions should be sent to the publishers, North-Holland Publishing Company, P.O.Box 103, Amsterdam or to any subscription-agent. Subscriptions for U.S.A. are to be sent exclusively to Interscience Publishers, Inc., 250 Fifth Avenue, New York, 1 N.Y.

No part of this issue may be reproduced in any form, by print, photoprint, microfilm or any other means without written permission from the publisher. Reprints, photoprints or microfilms are obtainable at cost from the publisher.

NUCLEAR INSTRUMENTS 1 (1957) 233–241; NORTH-HOLLAND PUBLISHING CO. – AMSTERDAM

EDITOR'S NOTE

The field of controlled fusion reactions and its possible technical applications for energy production has become one of the most challenging research tasks of our time. Great efforts are presently being made in many countries in order to try to solve all the intricate problems which are too well known to exist before the goal is within sight. Although progress undoubtedly has been made already very little has been published in the open litterature because of publication restrictions. The tendency in the policy of releasing scientific results in this field is fortunately improving at present and we probably can expect some declassification of papers to occur within the near future. It is very much the Editor's hope that this declassification policy will be shaped as liberal as possible. Nuclear Instruments will give a certain priority for papers related to the field of controlled fusion reactions. In the following article we present the first paper on this field published in this journal and the Editor's hereby kindly invites all colleagues from other laboratories to submit their results for publication in Nuclear Instruments.

Uppsala, July 27, 1957

FUSION EXPERIMENTS IN DEUTERIUM PLASMA

SETH BERGLUND, ROBERT NILSSON,
PER OHLIN, KAI SIEGBAHN, TAGE SUNDSTRÖM AND SVEN SVENNERSTEDT

Institute of Physics, Uppsala, Sweden

Received 27 July 1957

An experimental set up for studying fusion reactions and other features of a hot plasma is described. A low inductance condensor bank of 60 μF has been used and high current discharges in deuterium through straight tubes have been studied. The neutron production was found to be rather critically dependent on many factors. Two new fenomena have been observed: neutrons may appear already in the first pinch and furthermore, a high frequency oscillation in the plasma may occasionally be excited just after the pinch has been formed with a subsequent, strongly enhanced emission of neutrons.

1. Introduction

Although it is known that considerable work on producing fusion reactions in deuterium gas has been carried out at several laboratories very little has been published in this field. In fact, the only publications up to now are those of Kurchatov[1]) and Artsimovich *et al.*[2]). In addition to this, results were communicated at the third international conference on ionization phenomena in gases. (Venice, June 11–15, 1957) by Colgate *et al.* (Livermore), Allen and Curran (Aldermaston) and by the present authors. The method used in these experiments consists of passing a heavy current (some 100 kA) from a suitable condenser bank through a cylindrical discharge tube containing deuterium at a pressure of some

[1]) I. V. Kurchatov, Atomnaya Energiya **3** (1956) 65.

[2]) L. A. Artsimovich *et al.* (A. M. Andrianov, E. J. Debrokhotov, S. Yu Lukyanov, I. M. Podgornyi, V. I. Sinitsyn and N. V. Filippov) Atomnaya Energiya **1** (1956) 84.

tens of microns. The pinch effect in the gas is studied by oscillographic recordings of voltage, current and dI/dt and by photographic methods. Neutrons are detected by scintillation counters and activation of silver foils.

The results of the present work, which was started in the beginning of 1956, are largely in agreement with those obtained by the above mentioned authors. In addition some new interesting effects have been observed, however, and although we have found them quite recently and the experimental material is fairly scanty so far, we believe that the new fenomena are of such significance that we would like to report on them on this stage of the experiments.

2. Apparatus

Pulsed high current discharges in gases require some means of storing electric energy, e.g. by the charging of condensers. The current aimed at in the present experiments was of the order of megaamperes, and to reach this with a reasonable total capacitance and not too high a charging voltage, the condensers and the discharge arrangements both had to be carefully designed.

A very low inductance of the condenser bank was desirable, not only in order to reach a high short-circuit current but also to give a wide range of discharge times and to maintain a low inductance even with diminished capacitance. The insulation requirements grow rapidly with the applied voltage, and thus it is advantageous if the desired current can be reached without too high a voltage. Along with low inductance follow small stray magnetic fields, but stray electric fields that might interfere with the measuring devices should also be avoided.

The electrical properties must of course govern the design, but attention should also be paid to mechanical properties such as easy accessibility of the different parts for adjustments or replacements, since equipment of this kind is often charged very near the break-down voltage of the condensers.

A suitable standard condenser unit for our purposes was found in the ASEA condenser type CTOA11 illustrated in fig. 6. It has a capacitance of 0.5 μF, and a test voltage of 65 kV. Extensive tests were made to determine its qualities, especially its inductance. As this was considered somewhat high (400 mμH), arrangements were made to lower it to about 120 mμH. The outer connections could not be changed in this case, however. The later development showed that it is possible to lower the inductance of these condensers to at least 25 mμH.

At the first stages of the experiments a bank consisting of 40 standard condensers was used. These were closely packed around the discharge tube and connected by two parallel sheets of aluminium. In this case only air insulation was relied on, and the sheets were therefore 11 cm apart.

Simple as such an arrangement is, it is not practical for a large bank of condensers and this for several reasons: (a) As the condensers have

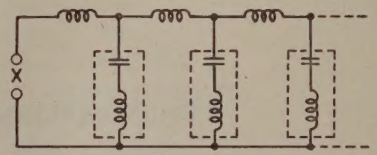

Fig. 1. Equivalent circuit of closely packed condenser bank. Details within dotted lines represent one or several condensers, equidistant from the discharge.

different coupling inductances to the centre, the equivalent circuit does not have the form of a simple series resonant circuit, but rather the form shown in fig. 1. (b) the arrangement is very rigid mechanically, and a faulty condenser is not easily replaced. (c) the total inductance is high, measured to be 50 mμH in the bank used, which limits the versatility of the experiments.

In view of the above, the optimum conditions for connecting the condensers of the main bank by means of parallel sheets were worked out. Circular symmetry taken for granted, the inductance of the sheets is obviously proportional to their separation. Good insulation between them is therefore necessary and polyethylene sheets should be the best material in most cases. The connection of the condensers disturbs the symmetry of the magnetic field

between the sheets, however, and makes the effective distance between them greater. This is illustrated in fig. 2, where (a) shows the physical

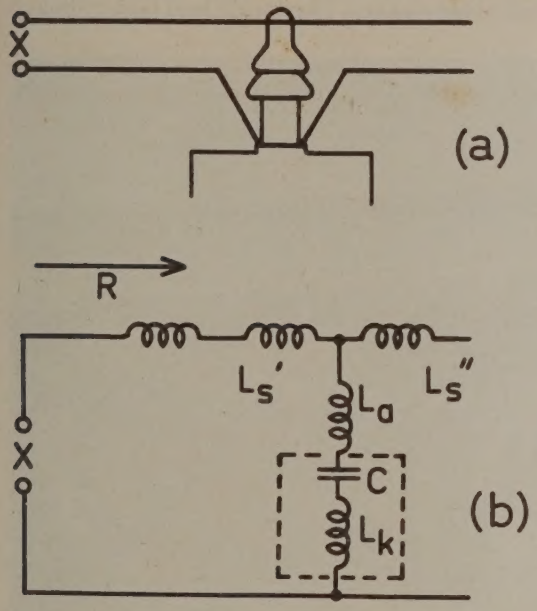

Fig. 2. (a) Physical appearance of a connection and (b) its electrical equivalent circuit.

appearance of a connection and (b) its equivalent circuit; the connection not only gives an extra inductance to the condenser itself, but also puts an extra inductance in the way of the current from condensers further away from the centre.

The conditions for minimum inductance can be calculated if it is assumed that an inner area of the sheets is free from connections: the area between r_0 and r_1 in fig. 3. There the distance between the sheets (d_1) and hence the inductance can be kept to a minimum, while a mean distance (d_2) is worked out within the outer area, between r_1 and r'_2, where the condensers are connected.

For the sake of simplicity the condensers are supposed to be connected along a circle with a radius r_2 such that $\pi(r'^2_2 - r_2^2) = \pi(r_2^2 - r_1^2)$; the area $\pi(r_2^2 - r_1^2)$ is of course given by the dimensions of the condenser units. Then a good approximation of the inductance is given by:

$$L = \frac{\mu\mu_0}{2\pi}(d_1 \ln r_1/r_0 + d_2 \ln r_2/r_1) \quad .$$

$dL/dr_1 = 0$ together with the known value of $\pi(r_2^2 - r_1^2)$ gives the radius r_1 for minimum inductance. r_1 grows of course with the difference between d_1 and d_2 and in most cases is so large that the condensers are nearly in parallel.

A detailed design following these lines was worked out for 120 condensers arranged in the same way as shown in fig. 4. With $r_0 = 20$ cm, $r_1 = 170$ cm, and $d_1 = 0.6$ cm, the total inductance calculated was 6.5 mμH.

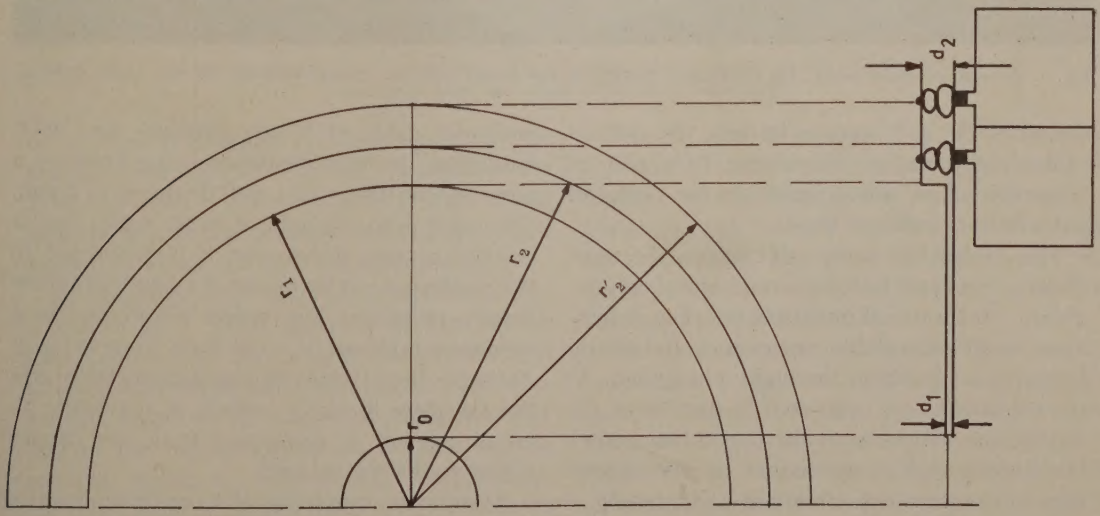

Fig. 3. Sketch showing coupling of condensers by means of circular, parallel sheets.

Although the above-mentioned design was satisfactory from the electrical point of view, it was abandoned for another alternative, a design with coaxial cables. This is the design advantages of this design over the other should increase with the number of condensers.

The coaxial cables are constructed in the following manner. The central lead is an ordinary

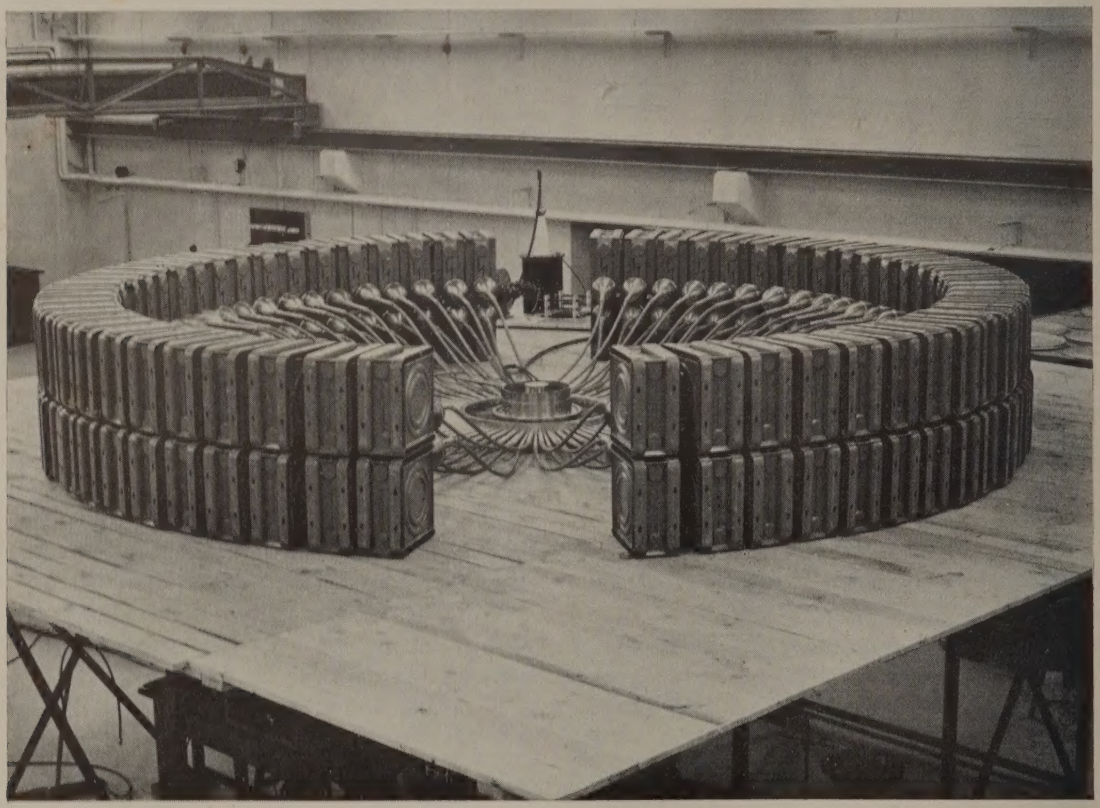

Fig. 4. View of condenser bank: 120 condensers. Length of the cables 165 cm. Outer diameter of the bank 420 cm.

shown in fig. 4–5, and as is seen, the coaxial cables are joined at the centre to a pair of concentric rings, which constitute the electrical poles of the condenser bank.

This design has many advantages, the most obvious perhaps being its mechanical adjustability. Its electrical qualitites are: low inductance, easily changeable capacitance and nearly complete screening of the high voltage end. As the condensers are connected in parallel at the centre, the short-circuit discharge time varies but little with the capacitance; it also follows that the equivalent circuit is very nearly a simple resonant circuit. Generally speaking the multiwire cable of 9 mm diameter and PVC insulation, the main insulation being, however, a polyethylene tube with a wall thickness of 2 mm. The outer lead consists of brass tubes and a braided copper sleeve, and it is connected to the condenser pot by means of a couple of hollow copper pressings. The entire connection to a condenser is shown in a cut-away view in fig. 6. As is seen, the polyethylene insulation also covers the porcelain insulator, which is necessary to guard against a spark-over from the copper sphere to the central lead.

Every unit, concisting of a condenser and its coaxial cable, has an inductance of 350 mμH,

which means 3 mμH for the entire bank of 120 condensers. Using the condensers with $L < 25$ mμH, mentioned above, and wider coaxial cables, it is possible to decrease this value to well below 1 mμH. The connections to the central poles contribute about 1.5 mμH to the total inductance, however. With a short circuit arrangement at the common centre of the rings a current of about 100 A/V has been reached.

A discharge tube and its connections are shown in fig. 7, where different relevant details are pointed out. Pyrex and quartz tubes of varying dimensions have been tested. They were broken, however, after some dischanges, partly due to the mechanical forces exerted by the external spark. A good electrical porcelain on the other hand proved to stand several hundreds of discharges. The best results so far have been obtained with a porcelain cylinder 60 cm long and 28 cm in diameter, with flat electrodes of aluminium, in the centre of which are placed porcelain slabs 11 cm in diameter.

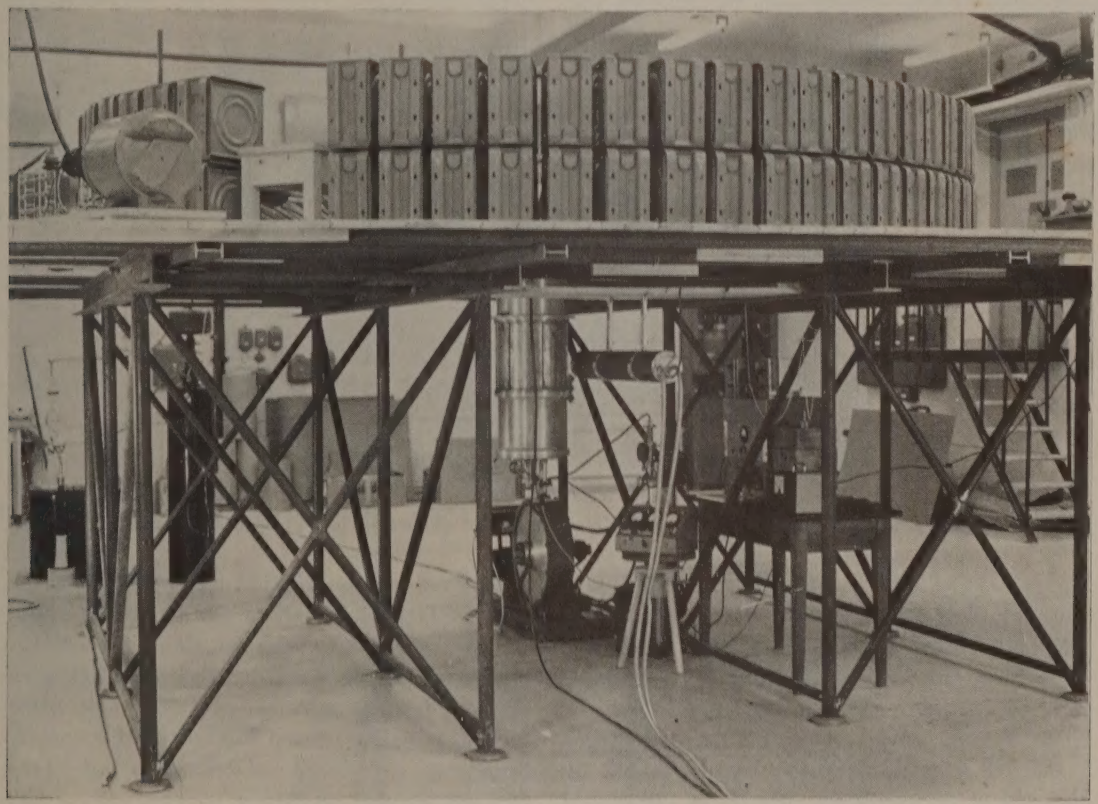

Fig. 5. Total view of the experimental arrangement. The condenser bank is placed on a table 2 m above ground with the discharge tube and other equipment underneath.

The D_2 gas is produced by electrolysis of D_2O of 99.7% purity and thus contains a small amount of H_2. The gas is let in through a palladium valve and is in this way freed from all components other than H_2 and D_2. During the experiments the gas has been kept streaming through the discharge tube.

The discharges were studied by oscillographic recordings of the time derivative dI/dt of the current through the tube and of the potential difference V between the electrodes. dI/dt was measured by means of a small pick-up coil, shown in fig. 7 and for the measurements of V[3])

[3]) N. Hyltén-Cavallius, Asea Journal 5 (1957).

a low resistance voltage divider was used. The current was calculated by numerical integration of dI/dt. Neutrons produced by fusion reactions in the gas were observed by means of a scintillation counter and oscillograph. The counter was

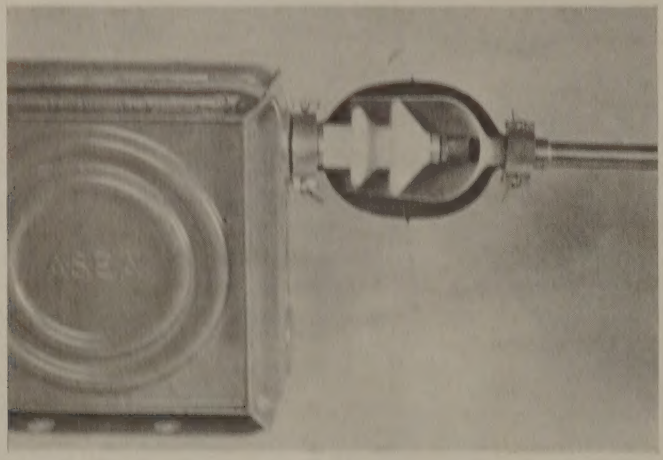

Fig. 6. The condensers have standard porcelain insulators which form part of the coaxial cables.

carefully shielded with 10 mm iron and 50 mm lead. V and dI/dt were recorded with a Tectronix 541 and for the neutrons a Tectronix 545 was used. Since only two oscillographs were available only two of these three measurements could be made simultaneously. The number of neutrons produced in each discharge was obtained by measuring the activation of a silver foil placed on the outside of the discharge tube. This device was calibrated using a Ra-Be standard.

3. Results

In order to get fusion reactions, a number of special precautions have proved to be necessary. The tube has to be cleaned very carefully both by ordinary chemical means and by electrical discharges. The outgassing by means of discharges is performed using the condenser bank and streaming D_2 gas. It has proved to be essential to carry out the outgassing at a voltage higher than the voltage used for production of fusion reactions. Usually the tube has been cleaned by several discharges at about 40 kV whereas the biggest neutron bursts appear at 25 kV or somewhat lower. Further, it is necessary to cover a region in the centre of the electrodes with some insulating material. The reason is probably that the pinch causes a strong heating of the central part of the electrodes if such covers are not used, giving rise to contaminations in the gas. In fact "focal spots" of a size of about 1 cm² are clearly visible at the centre of the electrodes (fig. 8). For protecting the electrodes, slabs of felspar porcelain are used. One other kind of porcelain tested caused the reactions to disappear completely probably because the melting point of its glazing was too low.

As mentioned before the design of the condenser bank and the spark gap gives them a very low inductance. The purpose of this is to make possible the use of big discharge tubes having a comparatively high inductance but still getting high values of the current and dI/dt. The actual tube (fig. 7), however, is of medium size and has too low an inductance to be used in connection with the spark gap of fig. 7. This gap inductance, 15 mμH, was therefore, in the present experiments, changed for another one with higher inductance (50 mμH).

Under the above-mentioned conditions reactions take place at pressures ranging from a few microns to about 50 microns; the best result so far has been obtained at about 10 microns i.e. at

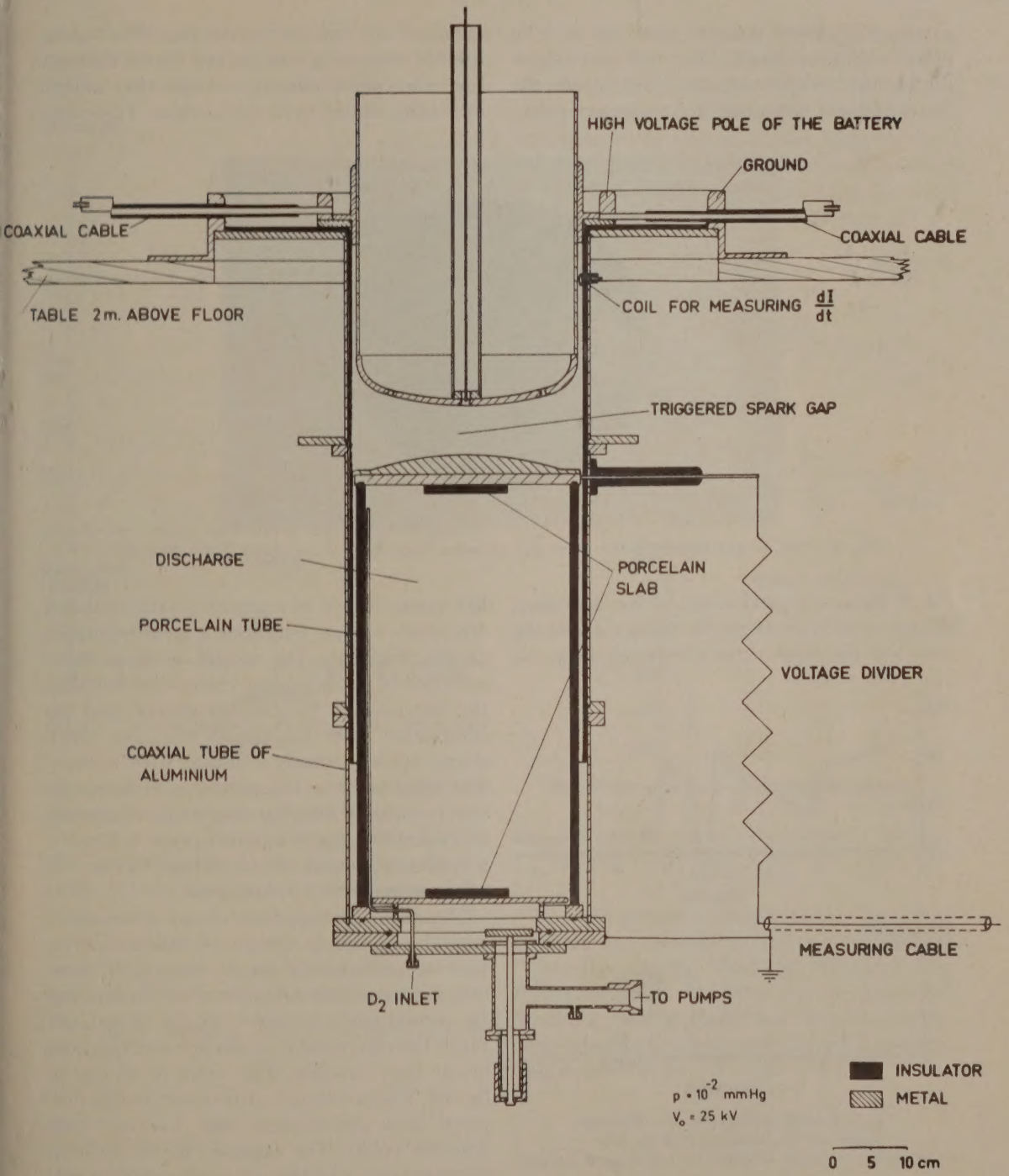

Fig. 7. Drawing to show the connection of the discharge tube to the condensers and a typical example of discharge tube arrangements.

a somewhat lower pressure than reported by other authors. Usually the neutrons appear during the second and the third pinch, the heaviest burst appearing at the second pinch. moment the contraction begins, manifesting itself by increasing voltage, and during the next 2 μs the pinch develops fully, the voltage increasing almost to its initial value. Thereafter

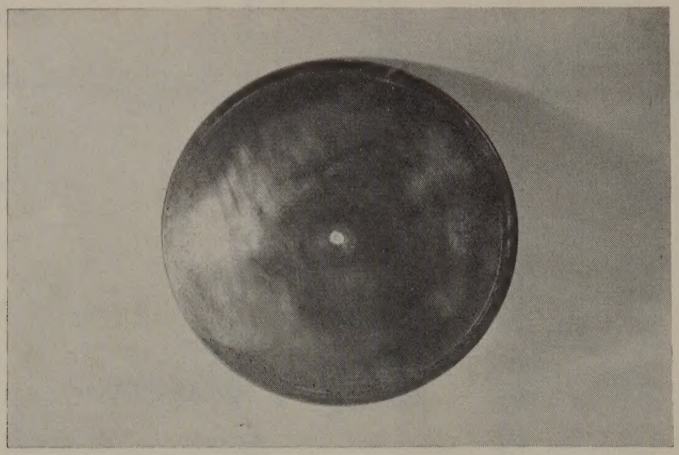

Fig. 8. After several discharges the pinch has caused a "focal spot" in the centre of the electrodes.

Fig. 9 shows a typical course of the discharge, the upper curve recording the voltage across the tube and the lower curve the signals from the

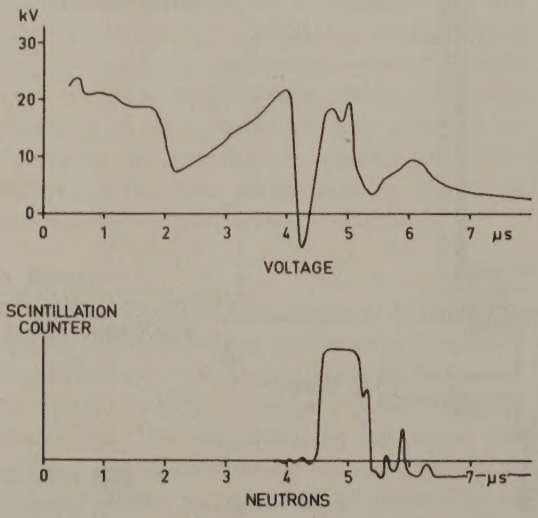

Fig. 9. Typical oscillograms of a discharge.
Upper curve: Voltage across the tube.
Lower curve: Neutrons recorded by scintillation counter.

scintillation counter. Starting from 25 kV the voltage drops below 10 kV within 2 μs. At this the voltage drops to a negative value within a few tenths of a μs, indicating a rapid expansion of the discharge. The second pinch is characterized by a much faster voltage increase than the first one and by the phenomenon that the contraction lasts for almost one μs, which shows up as a nearly constant high voltage. The third pinch is less pronounced, as can be seen from fig. 9. Simultaneously with the second pinch a strong neutron burst is recorded by the scintillation counter, followed by a weaker one at the moment of the third pinch.

The above development of the discharge is typical and well in agreement with the investigations published so far. In some cases, however, we have observed neutrons at the first and the second pinch instead of at the second and third. On one occasion neutrons even appeared at all three pinches. This event is shown in fig. 10. The occurrence of neutrons in the first pinch is a phenomenon that has not been detected before. For example, in the Russian investigations it turned out to be a definite rule that neutrons do not appear in the first pinch (see Artsimovich *et al. ibid.*). According to the

simple dynamic theory, however, it should be possible to get nuclear effects even in the first pinch, provided the longitudinal electric gradient is made great enough, as has recently been pointed out by Burkhardt *et al.*[4]).

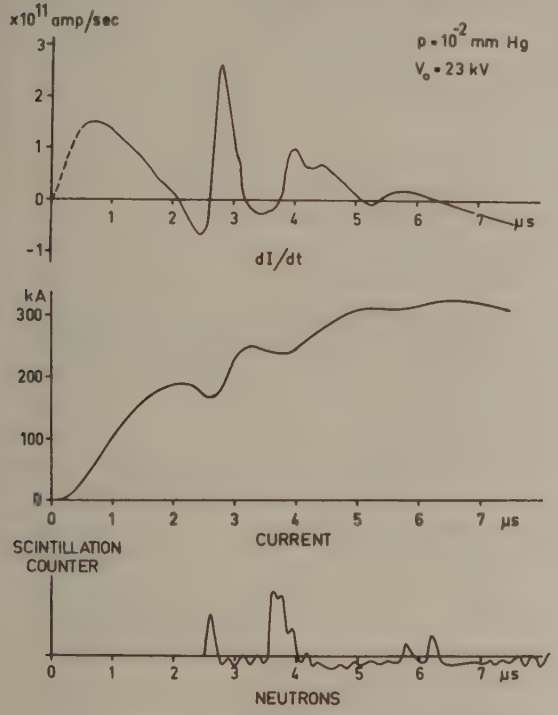

Fig. 10. Discharge, producing neutrons in *first*, second and third pinch.

Another new feature of great interest is illustrated in fig. 11. In the photographic record of the voltage the curve is actually missing for about one μs and this happened at the very moment when the second pinch should have occurred. Direct visual observations of the oscillograph screen revealed, however, that this part of the curve consisted of high frequency oscillations, too fast to be recorded by the film. The frequency is estimated to be 3–4 Mc/sec and the amplitude 10–15 kV. This oscillation was accompanied by a burst of more than ten times the mean value of the neutrons normally present. A few other events of the same kind have been recorded, but they were less pronounced.

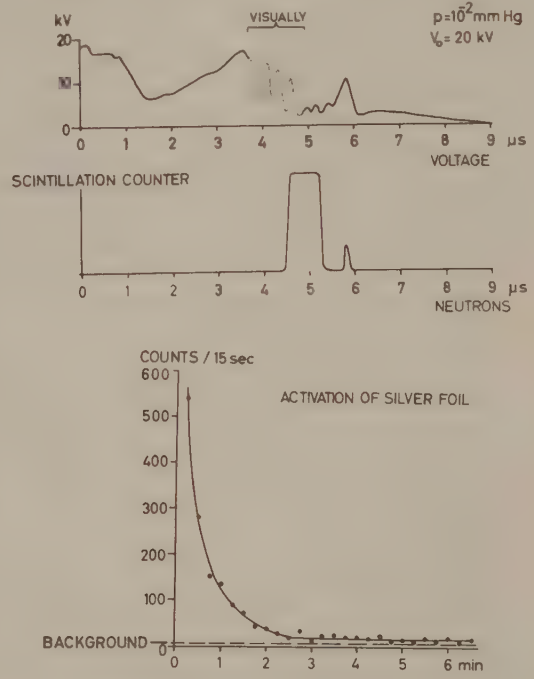

Fig. 11. Discharge having a high frequency oscillation 3–4 Mc/sec) in the second pinch and a very high neutron yield. See text.

We wish to express our gratitude to the ASEA company and specially to H. Liander, U. Lamm (Västerås) and G. Rydbeck (Ludvika), N. Hyltén-Cavallius, H. Witt and G. Engström (Ludvika) and B. Zetterstedt (Stockholm) for very valuable financial and technical support.

[4]) Louis C. Burkhardt *et al.*, Journ. Appl. Phys. **28** (1957) 519.

NUCLEAR INSTRUMENTS 1 (1957) 242–250; NORTH-HOLLAND PUBLISHING CO. – AMSTERDAM

TRANSFORMATION D'UNE FOCALISATION DE PREMIER ORDRE EN FOCALISATION DE DEUXIÈME ORDRE EN SPECTROGRAPHIE MAGNÉTIQUE A CHAMP HOMOGÈNE

R. J. WALEN

Laboratoire de l'AIMANT–PERMANENT

Centre de Recherches du C.N.R.S. — Bellevue (S.&O.) — France

Received 17 April 1957

The described magnetic lens, which corrects for the aberrations of a homogeneous magnetic field spectrograph, is inserted together with the defining slit of the beam of charged particles. This lens is essentially correct for a narrow gap such as used for the focalisation of heavy particles, when axial aberration remains un important.

1. Introduction

La spectrographie magnétique des particules lourdes: p, d et, plus particulièrement ici, α s'effectue aujourd'hui concurremment par plusieurs types d'appareils qui se distinguent essentiellement par le genre de focalisation qu'ils donnent et par la grandeur de la gamme d'énergie admissible au cours d'un enregistrement unique.

En général, et quel que soit le type adopté, un degré de focalisation élevé s'obtient au détriment de l'étendue de la gamme d'énergie pour laquelle les aberrations restent inférieures à une limite donnée. Un spectrographe à 180° à champ homogène, par ailleurs, permet d'enregistrer une gamme très étendue d'énergie, mais ne comporte qu'une focalisation radiale de premier ordre, celle axiale étant nulle. Un pouvoir séparateur élevé ne s'obtient alors qu'en limitant les angles solides.

Les appareils à focalisation radiale de second ordre par contre donnent un pouvoir séparateur élevé, mais dans une gamme d'énergie dont l'étendue varie en gros suivant l'inverse du carré de l'angle solide.

En développant en série l'expression de l'aberration, et tenant compte du fait que dans la spectrographie α les champs magnétiques élevés nécessaires ne s'obtiennent qu'au moyen d'entrefers étroits, on trouve que le terme prépondérant de cette aberration est celui qui contient le terme radial (angle ψ_r), la focalisation axiale n'intervenant pratiquement que dans l'expression de l'angle solide. Comme la focalisation axiale ne permet en fait que de gagner sur l'intensité un facteur de l'ordre de 2 dans le cas des sources linéaires, le facteur important dans l'obtention d'une résolution élevée est donc la focalisation radiale, du moins dans le cas spécifique de la spectrographie des particules lourdes d'origine nucléaire.

Jusqu'à ici le choix d'un type de focalisation présentait un caractère définitif:

Ou bien un spectrographe possédait une focalisation faible (premier ordre, champ homogène à 180° ou à secteur) et une fonction d'aberration constante sur une gamme d'énergie couvrant tous les besoins.

Ou bien cette focalisation était d'ordre supérieur (champ non homogène à symétrie radiale ou champ homogène limité par des bords non linéaires) mais avec des restrictions importantes sur la gamme d'énergie des rayonnements enregistrables simultanément.

Les exigences expérimentales cependant ne permettent pas un choix aisé entre ces deux alternatives. Si dans la grande majorité des cas le dispositif à focalisation d'ordre supérieur est bien adapté à l'étude de la structure fine d'un corps émetteur donné, où la gamme d'énergie

couvre rarement plus de 1 MeV, la focalisation de premier ordre est au contraire indispensable là où un mélange de corps, reliés génétiquement ou par leur mode de production, doit être étudié dans son ensemble et couvre une large gamme énergétique. Ce dernier dispositif est encore utile pour les déterminations absolues d'énergie, car il ne nécessite qu'une mesure sans ambiguité d'intensité de champ magnétique.

Il a par suite paru utile de disposer d'un instrument unique couvrant ces deux besoins. Comme notre laboratoire est équipé d'un spectrographe à champ homogène et aimants permanents[1]), nous avons cherché à construire un dispositif transformant la focalisation radiale de premier ordre en focalisation de second ordre, facilement amovible suivant les besoins expérimentaux.

2. Disposition Générale

Il a paru que le dispositif le plus souple et le plus simple serait ici une lentille magnétique supplémentaire qui puisse se glisser dans l'entrefer de l'aimant existant.

Comme une telle lentille ne peut que donner des corrections de champ positives, il est clair que l'on ne peut pas annuler l'aberration caractéristique de la focalisation du premier ordre. Celle-ci consiste en effet en ce que la trajectoire moyenne (passant par le milieu de la fente) forme la "tête de ligne" et que les trajectoires écartées de celle-ci d'un angle ψ_r frappent la plaque photographique à une distance plus rapprochée de la source de la quantité $\rho\psi_r^2$. Pour annuler l'aberration, il faudrait donc diminuer localement la courbure de ces rayons extrêmes, donc y diminuer le champ, ce qui est impossible puisque cela impliquerait une augmentation de l'entrefer. Il ne reste donc que la solution contraire, c'est-à-dire, augmenter la courbure des trajectoires moyennes de façon à ramener leur intersection avec la plaque à l'endroit de la "queue de ligne". Ceci revient à imposer une correction égale à $\rho(\psi_{r_{max}}^2 - \psi_r^2)$.

Il est clair que l'on a intérêt à ce que les corrections apportées au champ soient les plus faibles possibles. Si on examine comment varie, en se déplaçant le long de la trajectoire, la correction locale de champ qui provoque sur la plaque un déplacement donné du point d'intersection avec celle-ci, on trouve que cette correction est évidemment infinie aux deux extrémités (source et plaque) et passe par un minimum au milieu. C'est l'endroit le plus "sensible" de la trajectoire à une correction. Il est par ailleurs évident que l'élément correcteur doit se confondre avec le diaphragme de définition du faisceau (fente) afin que, pour diverses énergies, les trajectoires les plus écartées passent par la région non corrigée du champ et la trajectoire centrale par la région de correction maximum. Ceci mène vers le dispositif schématique de la fig. 1 où les traits pleins correspondent aux trajectoires telles qu'elles doivent

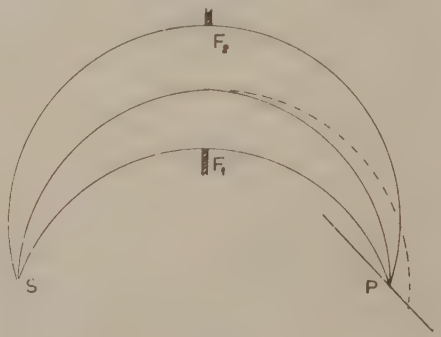

Fig. 1

être par intervention de la lentille correctrice, les traits pointillés indiquant les mêmes trajectoires en absence de correction. Nous avons précédemment indiqué[2]) l'avantage que ce dispositif procure en outre au point de vue de la position de la plaque photographique: celle-ci n'a plus besoin d'être inclinée par rapport aux lignes de champ afin de rendre lisibles les traces des particules, comme il est en usage dans les spectrographes à faible distance source-fente. La focalisation de second ordre comporte un angle radial bien plus élevé et toute la plaque doit

[1]) S. Rosenblum et B. Tsaï, C. R. Acad. SC. **224** (1947) 176.

[2]) R. J. Walen, Spectographe magnétique semi-circulaire de sources radioactives de faible activité spécifique, J. des Recherches du C.N.R.S. no. 30 (mars 1955).

être située dans le plan focal. L'inclinaison de 45° de la direction de pénétration des particules dans la plaque permet une lecture correcte des traces au microscope par suite du facteur de contraction.

3. Forme Générale de la Lentille Correctrice

Nous avons cherché à donner à l'élément correcteur de champ une forme qui puisse s'obtenir aisément par des procédés mécaniques normaux et qui se présente sous l'aspect général de deux lames plates en fer doux s'appliquant symétriquement contre les pièces polaires par leur côté plan (fig. 2).

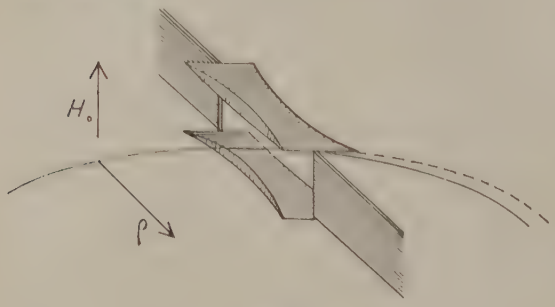

Fig. 2

Afin de pouvoir disposer du nombre nécessaire de paramètres d'ajustage, les surfaces de ces lames possèdent deux rayons de courbure perpendiculaires r_1 et r_2. Leur forme allongée n'est pas une nécessité à priori, mais facilite leur calcul et évite par là les tâtonnements. On est cependant limité dans ce sens par le fait que les lames doivent rester minces, afin que les rayons de courbure restent grands par rapport à leurs dimensions linéaires. C'est à cette condition en effet que les segments de cercle représentent de façon suffisamment approchée les portions de courbes du second degré nécessaires à l'obtention de la correction désirée.

4. Calcul de la Lentille Correctrice

Ce calcul se base sur les hypothèses suivantes:

(a) La perméabilité du fer est infinie.

(b) La portion de trajectoire située dans le champ correcteur est assez courte pour que la déviation supplémentaire qui en résulte puisse être assimilée à une déviation brusque qui a lieu au passage du plan médian de la lentille correctrice.

(c) Les lignes du champ magnétique restent pratiquement parallèles malgré l'insertion des lames correctrices supposées minces (en fait, le champ correcteur s'étend plus loin que le volume limité par les deux éléments correcteurs, mais le "smear out" qui en résulte ne modifie pas la valeur de $\int_{\text{traj.}} \Delta H \cdot ds$ pourvu que l'élément soit assez long et étroit).

(d) Tous les termes contenant ψ_r^n, $n > 3$, sont négligeables et les portions de cercle qui interviennent dans la construction de la lentille peuvent s'assimiler à la parabole tangente à ces cercles.

(e) Par suite de l'étroitesse de l'entrefer, la divergence axiale du faisceau est assez faible pour que les aberrations axiales soient négligeables.

La fig. 3 montre les notations. Les positions source (S) et image (I) sont déterminées par les trajectoires qui, passant par les bords de l'ensemble lentille diaphragme, ne subissent pas de

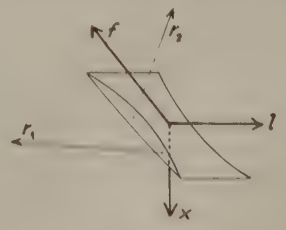

Fig. 3

correction. La distance SJ est un peu inférieure au diamètre.

On note:

f = distance comptée à partir du centre du diaphragme.

f_m = ouverture maximum de celui-ci (demi-longueur des lames correctrices).

l = largeur de la lame correctrice en f (l_0 au centre).

x = épaisseur de cette lame en f (x_0 au centre).

e = entrefer initial.

H = valeur du champ corrigé: $H = H_0 + \Delta H$.

r_1 et r_2 = rayons de courbure des surfaces limitant la lame correctrice.

ρ_0 = rayon de courbure de la trajectoire dans H_0.

$\alpha(f)$ = déviation supplémentaire de la trajectoire au passage de la lentille correctrice.

On trouve sans difficulté que les trajectoires doivent subir au passage de la lentille une déviation supplémentaire

$$\alpha(f) = \rho_0^{-2}(f_m^2 - f^2) \qquad (1)$$

pour qu'il y ait focalisation de second ordre.

On a d'autre part

$$l = l_0 + \frac{f^2}{r_1} \quad \text{et} \quad x = \frac{f_m^2 - f^2}{2r_2} \quad (\text{puisque } x(f_m) = 0)$$

et la déviation supplémentaire est donnée par

$$\alpha(f) = \frac{l}{\rho_0} \cdot \frac{\Delta H(f)}{H_0} \cdot$$

Si on admet que les surfaces polaires sont équipotentielles:

$$H_0 e = H(e - 2x) \quad \text{d'où} \quad \frac{\Delta H}{H_0} = \frac{2x}{e - 2x} \cdot$$

En égalant les deux expressions de α et exprimant tout en fonction des paramètres géométriques:

$$e - \frac{f_m^2 - f^2}{r_2} = \frac{\rho_0}{r_2}\left(l_0 + \frac{f^2}{r_1}\right) \cdot$$

D'où, par identification des termes constants et variables:

$$r_1 = \rho_0 \quad , \quad r_2 = \frac{f_m^2 + \rho_0 l_0}{e} \cdot \qquad (2)$$

Un compromis constructivement commode consiste à prendre $r_2 = \rho_0$ ce qui donne

$$l_0 = e - \frac{f_m^2}{\rho_0} \qquad (l_{max} = e) \cdot$$

La fig. 4 montre les résultats obtenus expérimentalement avec une lentille correctrice construite suivant ces données. Au moyen d'un diaphragme à 5 fentes séparées, le faisceau a été divisé en 5 nappes et enregistré sur plaque inclinée. Le cliché (a) montre les propriétés focalisatrices classiques du champ homogène en absence de lentille correctrice, et le cliché (b) avec correction (Source: dépôt actif du thoron, un tirage contrasté des clichés faisant ressortir

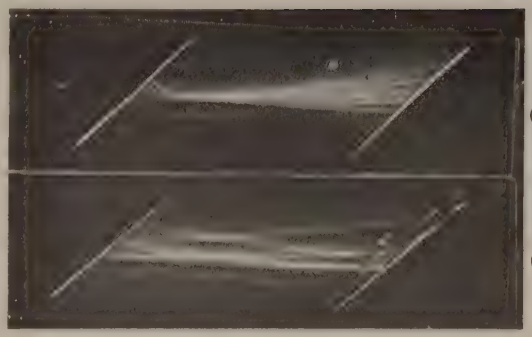

Fig. 4

au mieux ce qui se rapporte à la ligne la plus intense).

On voit que les simplifications admises sont valables. Les données numériques étaient:

$\rho_0 = 260$ mm, $H_0 = 13\,500$, $f_m = 30$ mm, ouverture utile du diaphragme: 52 mm (ouverture radiale du faisceau: 0.2).

Par suite du champ élevé, cependant, une légère correction avait été apportée à la largeur de la lentille:

$l_0 = 12.5$ mm au lieu de 11.5 mm calculé, la différence ayant été évaluée au moyen de la courbe de perméabilité présentée par le fer (armco) de la lentille.

Le cas échéant, un tel essai permet d'apporter des corrections expérimentales à la lentille, mais ceci n'a pas été le cas ici, car l'élargissement par aberration a été trouvé inférieur à celui dû aux imperfections de la source.

5. Plan Focal

La lentille a été établie pour une énergie et un rayon de courbure donnés (E_0, ρ_0). En fait, la mesure d'un spectre couvre une certaine gamme énergétique et il reste à voir entre quelles limites on obtient une focalisation expérimentalement satisfaisante et comment il faut disposer la plaque photographique.

Par définition même, le plan focal se calcule au moyen des trajectoires qui passent par les extrémités de la lentille où le champ correcteur est nul, ce dernier étant chargé de focaliser au même point les autres rayons. La surface focale s'obtient ainsi au moyen de trajectoires circulaires et se ramène à un problème de géométrie

plane puisque les aberrations axiales sont négligeables.

Le théorème suivant, peu connu, permet de résoudre aisément la question:

soit un triangle SF_1F_2 (fig. 5), où SB_1 est la bissectrice intérieure de l'angle F_1SF_2 et SB_2 la bissectrice extérieure, où SH est la perpendiculaire abaissée de S sur F_1F_2, et où O est le milieu de F_1F_2.

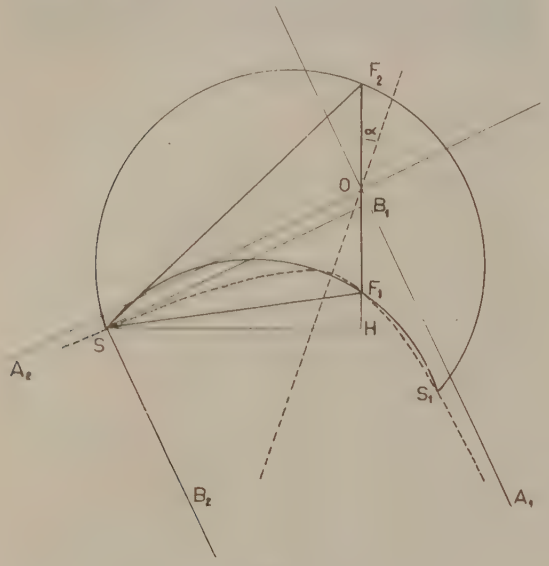

Fig. 5

Considérons les cercles de rayon R passant respectivement par les points S, F_1 et S, F_2 et se recoupant, suivant leur disposition, en 4 points, S_1, S_2, S_3, S_4. Si on fait varier R, ces 4 points décrivent 4 courbes qui dessinent dans leur ensemble une hyperbole équilatère complète (à deux branches), le raccordement des segments d'hyperbole ayant lieu pour $R = SF_2/2$, valeur du minimum (cas de la figure où $SF_2 > SF_1$). Les asymptotes sont les droites OA_1 et OA_2 parallèles à SB_1 et SB_2. Le demi-axe est égal à $OF_1\sqrt{\cos 2\alpha}$ où α, angle entre l'axe de symétrie d'une branche et la droite F_1F_2, est donné par

$$2\mathrm{tg}2\alpha = \frac{HS}{HO} = \frac{HF_1 \cdot HF_2}{HS \cdot HO} .$$

La fig. 5 montre seulement la disposition particulière des cercles qui présente un intérêt ici (les deux courbures étant dirigées dans le quadrant contenant H).

Pour appliquer le théorème précédent au plan focal du spectrographe, il faut se rappeler que l'emplacement le plus efficace de la lentille est celui où la source et l'image sont symétriques par rapport à cette lentille. Ceci ne vaut que pour le rayon de courbure ρ_0 pour lequel la compensation complète de l'aberration a été calculée. Ceci se traduit par les conditions:

$$\alpha = 0 \text{ c.à.d. } HS^2 = HF_1 \cdot HF_2 \text{ et } HO = \rho_0 .$$

En posant dans ce qui suit $\rho_0 = 1$ (unité de longueur), et en prenant H comme centre du système de coordonnées, on a la disposition de la fig. 6 avec $F_1F_2 = 2f_m$ et $SH = HS_1 = \sqrt{1 - f_m^2}$.

L'équation de la ligne focale est alors:

$$(1 - y)^2 - x^2 = f_m^2 . \qquad (3)$$

L'équation de la droite tangente en I est

$$y = -x\sqrt{1 - f_m^2} + 1 - f_m^2 \qquad (4)$$

et le rayon de courbure du cercle osculateur au même point est

$$R' = 2^{3/2} f_m^{-2} .$$

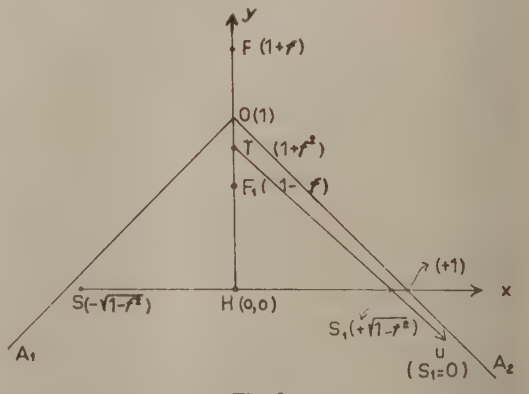

Fig. 6

Il est facile de voir que la droite tangente est, dans la pratique, une approximation suffisante de la ligne focale: les valeurs numériques utilisées dans l'appareil décrit ici sont $\rho_0 = 267$ mm et

$$2f_m = \frac{F_1F_2}{HO} = 0.224$$

d'où $R = 60$ m. Sur la longueur utile de la

plaque, qui couvre une gamme d'énergie de $\pm$ 15%, l'écart entre cercle osculateur et plaque photographique supposée fixée à une position moyenne parallèle à la tangente, n'excède pas 25 microns. Ceci est inférieur aux défauts de planéité d'une plaque nucléaire courante et aussi aux aberrations dont il sera question plus bas.

Le plan focal adopté est donc celui dont la trace sur le plan du spectrographe est une droite passant par les points $S_1(y = 0,\ x = \sqrt{1 - f_m^2})$ et $T_1(x = 0,\ y = 1 - f_m^2)$ (fig. 6).

6. Dispersion et Aberrations

La dispersion se calcule au moyen des mêmes trajectoires extrêmes que celles qui ont servi à déterminer le plan focal.

Soit, pour des trajectoires de particules dont l'énergie diffère de E_0:

$$t = (E/E_0) - 1 \quad \text{c.à.d.} \quad 1 + t = \sqrt{\rho\rho_0^{-1}} \ .$$

On trouve analytiquement que les coordonnées du point focal sont, en fonction de l'énergie

$$x = \tfrac{1}{2}\left[\sqrt{(1 + f_m)(2t + 1 - f_m)} + \sqrt{(1 - f_m)(2t + 1 + f_m)}\right]$$

$$y = 1 - \tfrac{1}{2}\left[\sqrt{(1 - f_m)(2t + 1 - f_m)} + \sqrt{(1 + f_m)(2t + 1 + f_m)}\right] \qquad (5)$$

Soit S_1U l'axe des déplacements suivant le plan focal. Les longueurs comptées à partir de la ligne de référence située en S_1 sont données par

$$u(t) = [(x - \sqrt{1 - f_m^2})^2 + y^2]^{1/2}$$

ou, bien plus commodément, en utilisant la relation approchée (4):

$$u(t) = y\sqrt{\frac{2}{1 - f_m^2}} \ .$$

Cette expression peu pratique doit être développée en série, t et f étant relativement petits. On néglige les termes en f_m^4 et plus, ainsi que $f_m^2 t^2$ puisqu'ils sont du même ordre de grandeur que les différences, négligées, entre la ligne focale adoptée et l'hyperbole focale réelle. On trouve ainsi

$$u = \sqrt{2}\left(1 + \frac{f_m^2}{4}\right)\left(t - \frac{t^2}{2} + \frac{t^3}{2} - \cdots\right) \qquad (6)$$

L'appareil fera toujours l'objet d'un étalonnage expérimental, certaines incertitudes mécaniques ne permettant pas de connaître avec précision E_0 et ρ_0 qui interviennent dans cette équation (ρ_0 en tant qu'unité de longueur).

Une relation plus commode que (6) s'obtient en remarquant que le développement de $\ln(1 + t) = t - t^2/2 + t^3/3 - \cdots$ ne diffère de celui obtenu en (6) que de la quantité très faible $t^3/6$.

On peut ainsi écrire approximativement:

$$u = A \log E + B \qquad (7)$$

ce qui affranchit de la connaissance exacte de E_0 et ρ_0 et n'exige que deux lignes d'énergie connues pour déterminer les constantes A et B.

L'expérience a montré que l'équation (7) traduit les résultats expérimentaux avec la précision désirée, le terme $t^3/6$ négligé étant inférieur aux erreurs commises dans la lecture des lignes très écartées de la ligne centrale (et par là, généralement, peu intenses).

L'aberration est caractérisée par la largeur totale d'une raie donnée par une source linéaire lorsque l'énergie est différente de E_0. On calcule pour cela le point d'intersection avec le plan focal d'une trajectoire passant par un point f quelconque de la lentille et qui y subit au passage une déviation supplémentaire

$$\alpha(f, \rho) = \frac{f_m^2 - f^2}{\rho} \ .$$

Toutes réductions faites, on trouve que la distance du point d'intersection au point focal est, en première approximation

$$\lambda = \sqrt{2}(f_m^2 - f^2)t \ . \qquad (8)$$

Donc, pour $t > 0$, le point focal constitue la tête de ligne, et pour $t < 0$ au contraire, la tête de ligne est constituée par la trajectoire centrale ($f = 0$). La déviation donnée par (6) doit alors être diminuée de la largeur de raie.

En réalité, on ne peut utiliser la pleine longueur de la lentille. D'après les simplifications initialement admises, le point f_m marquerait une discontinuité dans la dérivée du champ magnétique, tandis qu'il y a évidemment un raccordement graduel entre la zone à champ corrigé et celle à champ constant; le champ

correcteur utilisable doit être limité par un diaphragme de dimensions $f_d < f_m$.

En notant $p = f_d^2 f_m^{-2}$, en négligeant les termes en f^2t^2 et f^2t^3, et en combinant (6) et (8), on aura pour les abcisses des têtes de ligne:

$$\text{pour } t > 0 \quad u_+ = \sqrt{2}\left[(1 + (p - \tfrac{3}{4})f_m^2)\, t - \frac{t^2}{2} + \frac{t^3}{2} \cdots\right]$$

$$\text{pour } t < 0 \quad u_- = \sqrt{2}\left[(1 - \tfrac{3}{4}f_m^2)t - \frac{t^2}{2} + \frac{t^3}{2} \cdots\right] \cdot \quad (9)$$

Dans le spectrographe actuellement utilisé, $p = 0.7$ et la différence de pente entre u_- et u_+ devrait être de l'ordre de 0.8%. Expérimentalement cette différence n'est pas facile à percevoir, car la définition qu'on adopte pour repérer une ligne vient obscurcir la question. En pratique on ne peut évidemment prendre la limite extrême d'une raie, ce qui manque de précision. Le repère le plus commode est la tangente au point d'inflexion, côte tête de ligne. Mais cette tangente est fonction de la position du maximum dans l'intervalle délimitant la ligne, et ce maximum est surtout fonction des trajectoires centrales qui forment un ensemble plus "compact". De ce fait, pour $t > 0$, on aboutit à une valeur de u intermédiaire entre u_- et u_+, et la différence entre les régions $t > 0$ et $t < 0$ est moins marquée que ne le laissent croire les équations (9). En pratique, l'équation (7) permet de couvrir toute la gamme d'énergie utile (c.à.d. $\pm$ 15% par rapport à l'énergie choisie comme unité) avec des erreurs n'excédant pas quelques keV aux extrémités, et qu'il est possible de corriger si nécessaire.

7. Aberrations Axiales

L'introduction de la lentille dans le champ homogène donne en principe une légère focalisation axiale, maximum pour les trajectoires centrales, presque nulle pour celles extrêmes. Expérimentalement, l'effet est si faible que l'on peut admettre que sa variation avec l'énergie est négligeable et qu'il n'intervient donc pas comme facteur variable dans l'expression de l'angle solide en fonction de l'énergie.

8. Angles Solides

La variation de l'angle solide avec l'énergie est moins simple dans le montage avec focalisation corrigée que dans la spectrographie à champ homogène, où l'angle total radial $2\psi_r$ est constant (si la fente est suffisamment rapprochée de la source) et où seul l'angle total axial $2\psi_a$ varie ($\psi_a \approx \rho^{-1}$).

De simples considérations géométriques montrent que la disposition spéciale du diaphragme donne ici un angle ψ_r fonction de l'énergie de la particule. Un développement limité, de précision expérimentale satisfaisante, donne

$$2\psi_r = f_d\left(1 + \tfrac{1}{2}\frac{\rho_0}{\rho} + \tfrac{1}{2}\frac{\rho_0^2}{\rho^2}\right) \cdot$$

L'angle solide total $\Omega = 4\psi_r\psi_a$, rapporté à sa valeur pour l'énergie où la focalisation est exacte ($t = 0$) est par conséquent:

$$\frac{\Omega}{\Omega_0} = \tfrac{1}{2}\frac{\rho_0}{\rho} + \tfrac{1}{4}\frac{\rho_0^2}{\rho^2} + \tfrac{1}{4}\frac{\rho_0^3}{\rho^3} = 1 - \tfrac{7}{8}t + \tfrac{29}{32}t^2 - \cdots \quad (7)$$

9. Dispositif avec Source Étendue

La source ponctuelle ou linéaire est une abstraction qui ne se rencontre pas expérimentalement. La symétrie qui existe entre image et source dans le cas d'une focalisation radiale d'ordre supérieur montre qu'une source étendue doit être disposée conformément à la fig. 7, et

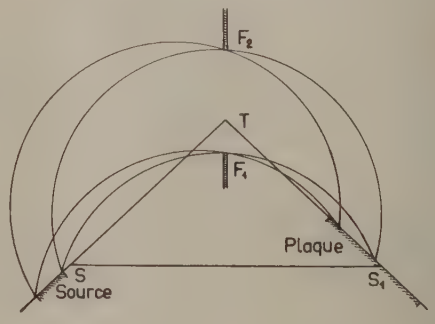

Fig. 7

que le rayonnement part donc à 45° de la surface. Pour les mêmes raisons, l'emplacement de la source n'est pas très critique: des petits déplacements suivant la droite S_0T, à partir de la position calculée, conservent constante la somme des distances: source-milieu fente + milieu fente-plaque, et laissent intacte la focalisation de second ordre.

La plupart des sources radioactives sont obtenues par volatilisation thermique et, de ce fait, n'ont pas des limites nettement définies. Il est alors nécessaire de disposer devant elles une fente de définition. Pour des raisons expérimentales, cette fente ne peut posséder des bords minces (diffusion, absorption) comme une fente optique, et aura de préférence des bords formés de deux fils parallèles. La surface utile de la source est alors variable avec l'énergie.

Si le plan passant par les axes des fils est parallèle à celui de la source, comme défini ci-dessus, et si on note

$$a = 2 \frac{\text{diamètre des fils}}{\text{distance de leurs axes}},$$

on trouve, en première approximation, que la largeur utile de la source, prise en valeur moyenne pour tous les angles de départ permis par ψ_r est

$$d/d_0 = 1 - a\rho/\rho_0 \cdot$$

Si la source a une activité superficielle constante, l'angle solide donné par (7) est modifié par la présence de la fente et devient:

$$\frac{\Omega'}{\Omega_0} = 1 - \tfrac{1}{8} \frac{7 - 3a}{1 - a} t + \tfrac{1}{32} \frac{29 - 11a}{1 - a} t^2 \quad \ldots \quad (8)$$

Une certaine indétermination expérimentale existe donc sur Ω' puisque la portion utile de la surface de la source est variable (faiblement) avec l'énergie et qu'il est difficile d'obtenir une densité d'activité très constante, à moins de volatiliser avec un rendement très mauvais.

S'il est important d'obtenir une précision élevée sur l'intensité, on peut sacrifier un peu sur la résolution et disposer le plan source et le plan de la fente de définition de celle-ci parallèlement à la ligne SS_1 (fig. 7). L'équation (7) est alors assez exacte, car la surface utile de la source ne varie plus que très faiblement avec l'énergie.

10. Discrimination et Angle d'Arrivée

L'interprétation d'un spectre se complique toujours du fait qu'en dehors du rayonnement désiré la plaque reçoit un rayonnement parasite: particules ralenties, diffusées, contamination radioactive dans l'entrefer. Dans la mesure du possible, il faut pouvoir discriminer entre les "bonnes" traces et les mauvaises. Pour les particules qui proviennent de la source et qui y ont été modifiées in situ (freinage dans la source, diffusion par les bords de la fente de définition) le problème n'est pas d'ordre spectrographique et ne relève que de soins expérimentaux. Pour les contaminations, il est possible d'après l'aspect de la trace (direction d'arrivée, longueur) de juger dans une certaine mesure si celle-ci provient de la source ou non. Comme chaque point de la plaque ne peut recevoir en principe que des particules de parcours et de domaine angulaire donné, on peut appliquer un double critère de sélection.

Dans le dispositif décrit ici, il faut noter que la trace a une composante parallèle à la surface de la plaque qui varie suivant ρ^2 (tandis que cette variation est en ρ^3 dans la spectrographie à 180° sans correction de champ).

La discrimination en direction est plus difficile que dans le cas du champ constant où la plaque inclinée par rapport aux lignes de force (et presque parallèle aux surfaces polaires) montre nettement si la direction de la particule est comprise ou non dans l'angle d'arrivé $\pm \psi_r$. Mais ceci n'est possible que parce que cette plaque n'est pas située dans le plan focal, mais le coupe seulement.

La nécessité, lors d'une focalisation de second ordre, de placer la plaque entièrement dans le plan focal est le prix inévitable d'une ouverture angulaire et d'une résolution augmentées. Le rôle de la discrimination par la longueur est alors prépondérant.

11. Construction

La fig. 8 montre la construction du bloc source-lentille correctrice-plaque réceptrice tel qu'il est en service au laboratoire depuis une demi-année.

La forme générale résulte du fait que la boîte à vide, disposée entre les pièces polaires, ne possède que des ouvertures de largeur très limitée par où doivent s'introduire les appareils. De plus, pour assurer la reproductibilité des résultats, les trois constituants: porte-source,

porte-plaque et lentille doivent former un tout indéformable. L'expérience ayant montré que les minces lamelles correctrices ne pouvaient

Fig. 8

être extraites du champ magnétique assez élevé (14 000 gauss) sans déformation, celles-ci sont noyées et soudées dans de fortes lames de laiton qui assurent la rigidité mécanique voulue.

12. Conclusions

En tant que dispositif à focalisation d'ordre supérieur, l'ensemble décrit ici souffre évidemment de quelques désavantages par rapport aux spectrographes construits spécialement dans ce but (par ex. à champ en $R^{-\frac{1}{2}}$ et focalisation double à $\pi\sqrt{2}$). Le plus notable est l'absence de focalisation axiale qui fait perdre un facteur de l'ordre de 2 en intensité. Mais la gamme d'énergie, pour laquelle la focalisation radiale est bonne, est à peu près identique à celle donnée par un spectrographe à focalisation à $\pi\sqrt{2}$ et de même ouverture radiale. Il est par ailleurs avantageux de pouvoir alterner sans difficulté des expériences à grande bande d'énergie et d'autres à focalisation élevée destinées à mieux préciser une structure fine. Le dispositif additionnel de focalisation est de construction aisée et est particulièrement facile à retoucher. A ce point de vue il ne peut être comparé aux spectrographes où la focalisation est obtenue par une taille précise des pièces polaires toutes entières, opération mécaniquement très délicate.

Je remercie Monsieur Salomon Rosenblum, Directeur du Laboratoire, pour les facilités accordées à ce travail et pour les discussions lors de sa réalisation.

NUCLEAR INSTRUMENTS 1 (1957) 251–252; NORTH-HOLLAND PUBLISHING CO. – AMSTERDAM

ON THE POSSIBILITY OF APPLYING TROCHOIDAL ORBITS IN BETA-SPECTROSCOPY

K. G. MALMFORS

Nobel Institute of Physics, Stockholm

Received 20 May 1957

The trochoidal motion of beta-particles in a strong slightly inhomogeneous magnetic field was first studied by Thibeau[1]). The following two essential properties were pointed out. (1) Positive and negative particles are directly separated since the drift motion goes in opposite directions in the two cases. (2) The transmission can be made very high because a large fraction of all particles emitted from a point source take part in the trochoidal beam. An instrument was constructed with the purpose of separating positive and negative electrons. No attempts seem to have been made to use a trochoidal beam for quantitative beta-spectroscopy.

It is the purpose of this paper to point out briefly the possibility to construct a beta-spectrometer according to this principle, where the high transmission can be combined with a fairly good resolution, by measuring the β-energies by the time-of-flight technique. It seems likely that the direct separation of positive and negative electrons may be of special importance for the construction of a pair-spectrometer.

Let us consider a magnetic field of the same general shape as in a double focussing spectrometer and so strong that the radius of curvature of the beta-particles is small compared to the radius of the magnet. All electrons which start from a point source and move in the symmetry plane of the magnet constitute a trochoidal beam, which drifts round the magnet at constant mean radius. Due to the fact that the magnetic field decreases in the radial direction the orbits are stable around the symmetry plane. Thus the general type of motion will be an oscillation through the symmetry plane superimposed on the trochoidal motion. Some calculations of the properties of such orbits[2]) give as the main result the drift velocity v.

$$v = \frac{m_0c^2}{e} \cdot \frac{n}{H \cdot r} \cdot E \cdot \frac{1 + E/2}{1 + E} \cdot \left(1 + \frac{2n}{4} \cdot \frac{n^2}{r^2} \cdot \frac{z^2}{r^2} \cdot \ldots\right)$$

where n defines the gradient of the magnetic field, $H \propto r^{-n}$, H is the magnetic field strength in the symmetry plane at radius r, E is the particle energy in units of m_0c^2. The parentheses gives in the first approximation the influence of the oscillation amplitude, z, on the drift velocity. It is an important feature that the drift velocity is independent of the amplitude if $n = 2$.

The energy of beta-particles can be determined by measuring the drift velocity by the time-of-flight technique. The total flight time over one half turn round the magnet can be made of the order of a microsecond and can be measured with a resolution of a few millimicroseconds by means of fast scintillation counters. Another factor which puts a limit to the resolution is the fact that, due to different starting directions, there is a relative uncertainty in the flight path, which is of the order $\rho/\pi \cdot r$ where ρ is the radius of curvature.

The application of the time-of-flight technique to beta-spectroscopy may offer good possibilities in connection with the study of gamma-radiation from charged particle reactions, if the incoming particle beam is pulsed, as is for instance the case if a cyclotron is used. Some

[1]) J. Thibeaud, Nuovo Cimento 15 (1938) 313.

[2]) *Cf.* H. Alfvén, Ark. f. Mat., Astr. o. Fys. 27A (1940) no. 22.

conceivable properties of a time-of-flight pair-spectrometer are mentioned below.

(1) The target can be placed quite close to the pair converter, as the gamma-beam need not be collimated.

(2) If the converter has the shape of a thin foil placed in the symmetry plane, its surface can be rather large, because the extension in the radial direction has no influence on the flight time if $n = 2$. The width of the foil in the azimuthal direction can be of the same order as the radius of curvature.

(3) Electrons and positrons move in opposite directions round the magnet and can be detected separately with two scintillation counters placed 180° from the converter.

(4) A large fraction of all pairs will be detected.

(5) A whole gamma-spectrum can be observed simultaneously by some multichannel method since the magnetic field should be kept at a constant value.

(6) The most direct method would be to measure coincidences between the two detectors but it seems also possible to use the whole range of energy distribution between the positive and the negative component of a pair. In principle an arrangement of the following type may be applicable for the purpose. The signal from the positron detector triggers the horizontal linear sweep of an oscilloscope and the signal from the electron detector triggers a similar sweep on the vertical plates. A third signal which indicates the time of the pair production is delayed and displayed as an intensity modulation of the oscilloscope beam. With such an arrangement different gamma-energies will give spots situated on different hyperbolas according to the approximate relation

$$\frac{1}{\tau_+} + \frac{1}{\tau_-} \approx F(E\gamma) \,.$$

(7) It seems possible that the resolution, which is mainly given by the accuracy of the time measurement, can be made better than 1% at low gamma-energies (< 10 MeV). At higher energies the accuracy decreases due to decreasing flight time and increasing radius of curvature, for a given size of the magnet.

Note added in proof

A preliminary experimental test has been made in a double focussing heavy particle spectrometer available at the Nobel Institute. A source of Bi^{207} was placed at one end of the spectrometer and the conversion electrons from the 1064 keV line were observed at the other end by means of a plastic scintillator. The delay was measured in relation to directly emitted gamma-radiation. Resolution, transmission and flight time at different magnetic fields were in good agreement with theoretical expectations. A magnet for a pair spectrometer is under construction.

NUCLEAR INSTRUMENTS 1 (1957) 253–258; NORTH-HOLLAND PUBLISHING CO. – AMSTERDAM

A DEVICE FOR THE PRECISION MEASUREMENT OF AN INHOMOGENOUS MAGNETIC FIELD

GUNNAR BÄCKSTRÖM

The Institute of Physics, Uppsala

Received 31 May 1957

A generator device has been constructed for measuring the field of a β-spectrometer, having a gradient of 1% per cm and a field range 10–300 gauss. A sensitivity of $1 : 10^5$ has been obtained.

1. Introduction

When trying to measure with some accuracy an inhomogenous field of the strength 10–300 gauss, one has a rather narrow choice of possibilities. The proton resonance, which is the most precise method in most other cases, fails here because of the low field and the existence of a considerable gradient.

Recently a method has been developed using the Hall effect in certain semiconductors. This possibility has been seriously considered, but it was found that the Hall generators now available are too strongly temperature dependent and yield too small voltages to produce an accuracy of better than $1 : 10^3$ in the present case.

The generator principle has been used in various modifications. The simplest device consists of a small coil rotated in the field with a constant speed, usually by a syncronous motor. The generated voltage is taken off by sliprings and brushes, rectified and measured. Alternatively, a commutator may be used instead of rectifying the induced voltage. With great care in stabilizing the rotational speed and measuring the voltage with a potentiometer, an accuracy of $1 : 10^3$ is just obtainable. Even if commutators are used, a rather heavy filtering of the voltage is essential, which slows down the accumulation of data. A field gradient is, however, of no objection here, as the generator measures a mean value over the volume of the coil.

A refined modification of the above method is introduced by mounting a second coil on the same axis, this one rotating in a fixed field. The rectified voltages are compared by means of a potentiometer. In this arrangement one has the obvious advantage of not having to stabilize the speed of revolution, why one expects somewhat higher precision, provided the fixed field and the one to be measured can be satisfactorily shielded from each other. From other points of view little advantage is gained. A common drawback of all methods which use rectification of the originally generated voltage, is that a certain current must be taken out and that the impedance of the rectifying unit may influence the measurements. For this reason it seems logical to keep the general idea of this last method, but to compare the two voltages before instead of after rectification, as has been done by Hedgran[1]). The subject of this article is the description of a similar apparatus with different technical approach, which has recently been constructed at this institute for use in conjunction with the big double focusing beta spectrometer. Further, a modification of the principle has been introduced, which may be used where an even higher sensitivity is desirable or where the demand on mecanical stability has to be kept more resonable.

2. Theory

A rigid, but arbitrary shaped coil, rotating in

[1]) A. Hedgran, Ark. Fys. B 5 (1952) no. 1.

a homogenous magnetic field B with the angular frequency ω generates a voltage $sBe^{i\omega t}$ where s is a constant of the coil for a given ω. This follows immediately from the magnetic laws, since the total linked flux varies sinusoidally. If we remove the stipulation that the field is homogenous the voltage is of course still periodical and we have the Fourrier expansion

$$E = s\overline{B}e^{i\omega t} + \overline{B}\sum_{\nu=2}^{\infty} a_\nu e^{\nu\omega t}$$

with a mean value $\overline{B}$ replacing B. It should be noted that the higher harmonic contents may become zero even in inhomogenous fields, i e. if there is homogeneity in each plane perpendicular to the coil axis.

In the experimental arrangement one coil is rotated in a reference field and the other in the unknown field, the voltages being added to give

$$\Delta E = s_1 B_1 e^{i\omega t} + s_2 B_2 e^{i(\omega t+\pi+\delta)} + \text{harmonics}$$

harmonic difference, where δ is kept very small. We find a minimum for $|\Delta E|$ at

$$B_2 - (s_1/s_2)\, B_1 = \Delta B = 0$$

and in the vicinity of this minimum we have for the fundamental voltage:

$$\Delta E = s_1 B_1 e^{i\omega t}(1 - e^{i\delta}) + (s_1 B_1 - s_2 B_2) e^{i(\omega t+\delta)}$$

$$\approx e^{i\omega t}\,[s_1 B_1 i\delta + \Delta(sB)] = s_1 B_1 e^{i\omega t}\left[i\delta + \frac{\Delta(sB)}{s_1 B_1}\right]$$

Fig. 1 shows a graph of $|\Delta E|$ as a function of

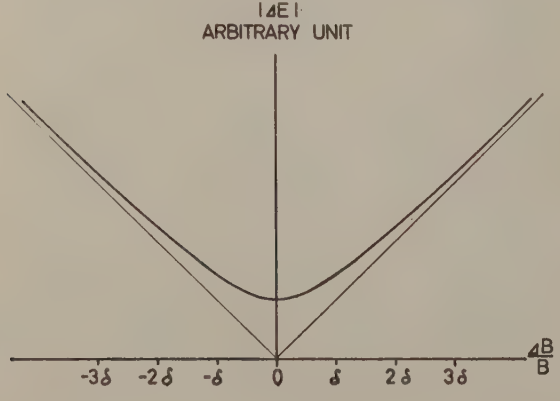

Fig. 1

$\Delta B/B$ in units of δ. Before anything may be concluded as to the accuracy in setting ΔB to zero, we must direct our attention to the important question of noise. One part of it has already been mentioned, i.e. the harmonic contents of the sum voltage. Although in principle this contributes only as a constant background to ΔE, it may in practice become inconveniently large and should be suppressed. This can be accomplished by using a frequency selective amplifier for ΔE and by shaping the reference field to ressemble the one to be measured. Furthermore, advantage should be taken of the fact that there is in general a way of placing the probe coil in the field so that the harmonics vanish to second order.

The next important source of noice are those phase angle variations, which are slow in comparison to the time of revolution. Looking at the expression for $|\Delta E|$ it is realized that the accuracy with which ΔB can be set to zero depends not only on the upper bound of $|\delta|$ but also on how constant δ is, since error signals from δ and B cannot be distinguished. Therefore, if other sources of error are disregarded it would be realistic to state that $\Delta B/B$ may be set less than $|\delta|$ max., i.e. that an increase of ΔE of the order of 40% may be regarded as significant. Further noise due to effects such as elastic mechanical vibrations, thermovoltages at the sliprings and pickup interference may be eliminated by good mechanical construction and by proper filtering.

The result is accordingly still valid, that for obtaining the sensitivity $1:10^4$, one must have $|\delta| < 10^{-4}$, where δ is the angle between two coils monted at the opposite ends of a rotating shaft. Since the rigidity of the shaft depends on its length some words should be said here about the factors determining this length. It has been shown by Hedgran[1]) that when the fields are "balanced", the measured field is a linear function of the ironfree reference field, as long as the stray field of the magnet is proportional to its field. Now this stray field cannot in general be checked to the accuracy for which the apparatus is designed so it is preferred to reduce the influence of the stray field to less than 10% of the total, or even

lower, since the reference field produces in the field of the magnet an extra gradient, which may sometimes be objectionable. However, there are certainly technical possibilities of maintaining $|\delta| < 10^{-4}$ over a shaft of several meters, so these conditions may in most cases be satisfied.

The setup so far discussed may loosely be described as a zero method for determining the field, but should strictly be spoken of as a minimum method. In practice we always have $\delta > 0$ and so have to operate at the bottom of the hyperbola of fig. 1, where the sensitivity is low and the noise level relatively high, as already mentioned. Furthermore, the error signal contains no information as to the sign of the deviation. If we modify the arrangement slightly, however, we may obtain a considerable improvement. We may add to one of the rotating coils a few extra turns so as to provide two sum voltages differring from each other by some units of $sB\delta$. These signals are amplified and rectified in two identical circuits and the outputs are fed to a difference bridge, which produces

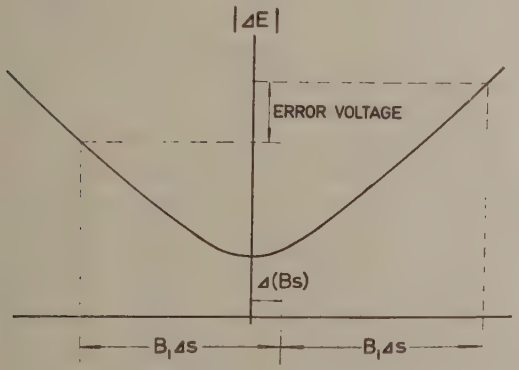

Fig. 2. A method of obtaining a linear error voltage.

the error signal. The situation is explained in fig. 2. The split coil generates two voltages $(s_1 + \Delta s)\, B_1$ and $(s_1 - \Delta s)\, B_1$ and the sums become

$$\Delta E_+ = e^{i\omega t}\,[isB\,\delta + \Delta(sB) + B_1 \Delta s],$$

$$\Delta E_- = e^{i\omega t}\,[isB\delta + \Delta(sB) - B_1 \Delta s].$$

If the first two terms are assumed to be small in comparison with $B_1 \Delta s$ the rectified difference comes out as

$$|\Delta E_+| - |\Delta E_-| \approxeq 2\,\Delta(sB)$$

i.e. the field error. We have accordingly gained a linear working region and a sign of the error signal. Further it should be noted that variations of δ yield essentially a second order contribution to ΔE_+ and ΔE_- and that even these small fluctuations tend to cancel in the difference. Also one finds that ΔE_+ and ΔE_- are nearly out of phase, so that if one of them is phase inverted before detection little filtering is necessary. The problem of zero adjustments is easily solved by feeding a common input ΔE_+ to both amplifiers and attenuating one of them to obtain zero.

3. Mechanical Construction

If the field sensitivity desired is $1 : 10^4$, the maximum tolerable torsion of the rotating shaft is about 5×10^{-5} radians and fluctuations due to displacement of the coil situated in the inhomogenous field must also be kept below this value. The immediate surrounding of the generating coils should be insulating in order to avoid troublesome eddy currents. Further, magnetic materials have to be kept sufficiently far from the fields so as not to yield unlinear contributions to their magnitude, why bearings should be placed if possible at points where steel is not objectionable. The torque exerted by the voltage collecting brushes should act over the shortest possible length of the shaft. Our construction, where the above principles have been followed, is shown in fig. 3. The ball bearings at the ends are specially made of austenitic stainless steel, having a low permeability. As a further precaution the outer ring is attached to the rotating part, whereby the remanency is kept small and is fixed relatively to the generating coil. Moreover the ring tends to screen the inner parts of the bearing from the outer field. For the insulating section was chosen an extremely rigid plastic material, "canvas isolite".

Because of workshop consideration the aluminimum shafts had to be made in halves of solid material, although tubes would have been

preferred, giving better stability for a given weight. The halves were joined by clamping together the carefully machined end surfaces and at one of these joints provision was made for angular adjustment by means of a micro-screw. At the middle of the shaft there is an axis of 20 mm stainless steel, where the motor torque is applied and where the sliprings and a ball bearing are placed. The aluminium and steel cylinders were connected by means of diametrical conical pegs. The brushes are standard quality carbon rods of the type used in DC motors.

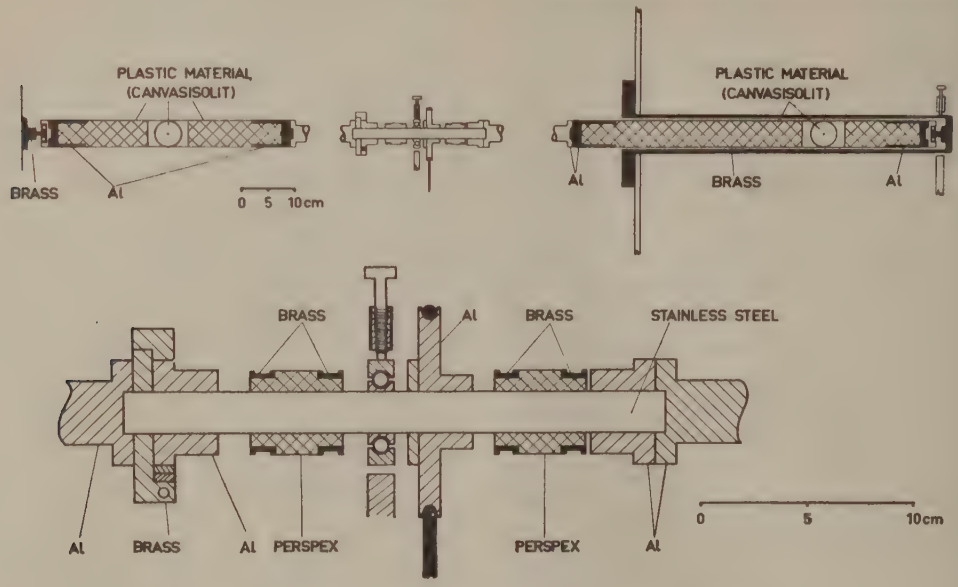

Fig. 3. The mechanical construction of the rotating shaft.

4. Electrical Construction

Obviously there are two ways of providing a reference field: by means of a permanent magnet or by an ironfree coil. If the first alternative is used, an accurately calibrated voltage divider is connected across one of the probe coils in order to equal the voltages generated. While this arrangement is admittedly easier to manipulate, it seems very difficult to effect a construction which is free of objections. The total resistance of the voltage divider has to be chosen rather high in order to avoid disturbing influences from contact resistances and from temperature variations of the coil. The temperature dependence of a permanent magnet necessitates thermal regulation, and even if it may be estimated that the stray field does not seriously penetrate into the air gap, it would be inconvenient to verify this experimentally. As an ironfree field is easier managed from all these points of view, this possibility was preferred.

As the unknown field in the present case is cylindrically symmetric, the rotating shaft was pointed to its axis, and as there exists a symmetry plane the shaft was kept within this plane in order to secure sinusoidal output voltage. The reference field could accordingly be made homogenous by using a Helmholz coil. With the two magnets connected essentially in series, the fields are already approximately balanced, the small correction being made with a variable shunt resistance over the spectrometer magnet.

The field due to the Helmholz coil is strictly proportional to the current only if its geometry is fixed, i.e. if its temperature is constant. As in our case only the frame of the coil is well cooled, it was preferable to correct for temperature dilation. Since an accurate potentiometer had to

be used anyway for control of the current, it was natural to base the correction simply on measurement of the voltage drop over the coil.

The probe coils, of 10 mm length and 50 mm outer diameter, were wound with 6000 turns each of enameled copper wire, and were found to give about 40 mV/gauss at 20 revolutions per sec. The cables from the coils to the collecting rings had to be drawn outside the shaft and were rigidly cemented to it and twisted in order to reduce pickup effects. When the minimum method is used the voltages are connected in series immediately at the brushes and the voltage difference led to the voltmeter by a coaxial cable. Since there is no objection to a load being applied to ΔE, the input cirquit is not critical, and thus the signal was applied directly to a two-stage amplifier with a twin-T filter in the feedback loop. This arrangement was followed by a commercial AC voltmeter which gave the reading.

No split coil was included in the above construction, but as it was of some interest to put this improvement to a practical test, some way of simulating the arrangement was searched for. To take out the smaller voltage from a voltage divider over the coil would be impractical, since it would require a specially wound constant resistor of several M Ω if temperature effects were to be avoided. On the other hand, if one notices that the small extra voltage $B_1 \Delta s$ is in phase with $B_1 s$ another solution presents itself. E_1 may be fed into a high impedance cirquit, properly attenuated and then added to ΔE_- to yield ΔE_+, after which one RMS value is subtracted from the other as described above. Now this is exactly what is done in the familiar phase sensitive detector, a cirquit which is treated in standard works on servomechanisms. The method outlined here can be thought of as rectifying the component of ΔE in the phase direction of E_1, the true error signal. A block diagram of our arrangements † is shown in fig. 4.

In the ΔE channel use was made of the previously built selective amplifier. A small load may in principle be applied to E_1, but a cathode follower to take out this voltage was

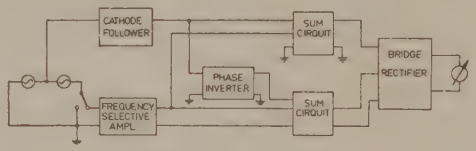

Fig. 4. Block diagram of the phase sensitive detector.

found necessary in practice. The zero adjustment was accomplished by shortcirquiting the input for ΔE. During measurements the real ΔE consists of a number of components: a fundamental frequency, harmonics, vibration frequencies and pick-up noise. The input that is to

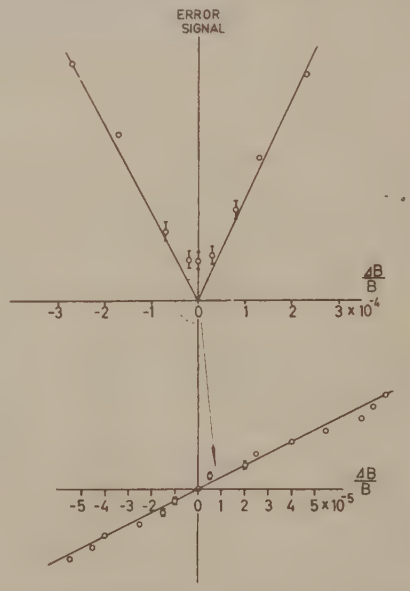

Fig. 5. Comparison between the minimum and null methods.

be simulated by the zero setting, should ideally contain all these components except one, i.e. the in-phase component of the fundamental voltage. That this is actually not fulfilled is not serious in the case of the harmonics, vibration and pick-up frequencies, because they are attenuated in the selective unit, and further, being negligible in the other channel, they do not contribute to the error signal on the average. The perpendicular component of ΔE is however also switched off,

† The author is indepted to Mr Mats Johansson for building these units.

which would be of no consequence in an ideal phase sensitive detector, but is here, since a selective amplifier has a frequency dependent phase shift, which may introduce an error, if the rotational speed is not sufficiently constant. Although in our case the relative error was found to be less than $\delta/5$ and so did not seriously impair the measurements, it is a definite disadvantage to have to check this point continuously. Because of this inconvenience the split coil system is recommended, since here the combination of voltages is made directly, thus removing the only hazardous part of the scheme. Alternatively a phase sensitive detector may be constructed in a symmetrical way, so as to shift the phases of V_1 and $-V_2$ to the same extent. It would also be possible to apply servo control to the phase angle δ.

The phase sensitive detector was tested at a stage when the mechanical apparatus was not yet in its final shape and was then found to yield an improvement by a factor or 5–10, (fig. 5) resulting in a sensitivity of $1 : 10^8$, which happened to be about the limit set by instability of current. Later on however, the figure 2–3 parts in 10^8 was attained even with the ordinary minimum method.

The method may no doubt be extended to orders of magnitude stronger or weeker fields and it seems suitable for magnet regulation. If a more localized measurement is necessary, this may be accomplished by giving the coil a special shape[8]).

The author wishes to thank professor Kai Siegbahn for clarifying discussion concerning this work.

[8]) N. Brown and J. Sweer, Rev. Sci. Instr. **16** (1945) 276.

NUCLEAR INSTRUMENTS 1 (1957) 259–267; NORTH-HOLLAND PUBLISHING CO. – AMSTERDAM

A HIGH OUTPUT D-D NEUTRON GENERATOR FOR BIOLOGICAL RESEARCH

A. C. van DORSTEN and J. H. SPAA

Philips Research Laboratories N.V. Philips' Gloeilampenfabrieken, Eindhoven-Netherlands

Received 7 June 1957

A description is given of an apparatus capable of producing a fast neutron flux exceeding 10^{10} neutrons per second from a D–D reaction. The set consists of a pressurized cascade generator and an accelerator tube with a rotary heavy ice target.

The rectifiers used are of the selenium type.

1. Introduction

In order to study the biological action of fast neutrons it is necessary to have available sources producing neutrons of sufficiently high energy at a sufficient rate and with a minimum of accompanying unwanted forms of ionizing radiation, such as excessive amounts of slow neutrons or gamma rays. For this reason natural neutron sources, e.g. RaBe or PoBe as well as photo-neutron sources have their limitations. Similar objections apply to the use of neutrons produced by nuclear reactors. In many cases it is also important to have mono-energetic neutrons.

In the range of the relatively high neutron energies the various types of heavy particle accelerators, such as cyclotrons, have served as the principal sources for experiments in general.

The use of exoenergetic reactions, where high energy neutrons are produced with relatively low energies of the bombarding particles, forms a more attractive method in a number of cases. Such reactions are e.g. the D–D, P–T and D–T reactions, of which the first one was chosen for the fast neutron generator described in this paper.

In order to serve the purpose indicated above, a total yield of the order of 10^{10} neutrons per second seemed a reasonable figure as a starting point for the design.

This yield, corresponding to that of about one kilogram Ra + Be, seemed attainable with a 1 MeV accelerator using the D–D reaction, provided the permissible load on a heavy ice target could be made as high as at least 300 watt.

The total number of neutrons per second produced by a deuteron beam of atomic ions in a thick D_2O ice target, is given by the expression:

$$2\int_0^U N\sigma(E)\mathrm{d}x, \text{ or } 2\int_0^U \frac{\sigma(E)}{\varepsilon(E)}\,\mathrm{d}E, \qquad (1)$$

in which U represents the deuteron accelerating potential, N the number of D_2O molecules per cc, $\sigma(E)$ the total D(d,n)He^3 cross-section for deuterons of energy E and $\varepsilon(E) = (1/N)\,\mathrm{d}E/\mathrm{d}x$ the molecular stopping power of heavy ice for deuterons.

Measured figures for $\varepsilon(E)$ are available from work of Wenzel and Whaling[1]) for protons in heavy ice. The value for deuterons can be derived from these data.

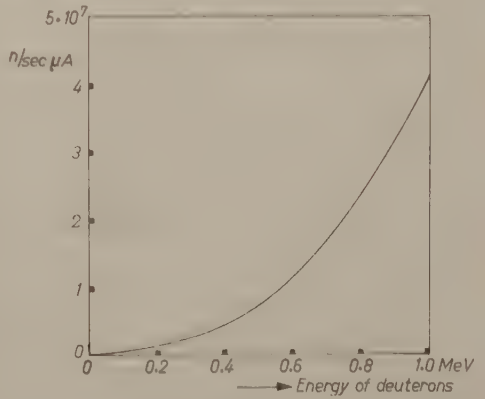

Fig. 1. Calculated neutron yield for an atomic deuteron beam on heavy ice.

[1]) W. A. Wenzel and W. Whaling, Phys. Rev. 87 (1952) 499.

The value for $\sigma(E)$ used was obtained by linear interpolation of the lowest values given by Hunter and Richards[2]). From the foregoing data we computed the curve for the total neutron yield as a function of the particle energy (fig. 1). From this curve it can be seen that for a yield of 10^{10} n/sec a deuteron beam current of 250 microampère is required at 1 MV, and of 420 microampère at 0.80 MV.

2. Alternative Targets

Alternative targets have been considered but were found to be less attractive. Possible targets are: D_2 gas target, heavy paraffin C_nD_{2n+2}, D_2O, D_3PO_4, NaOD, ZrD_2, TiD, ZrD, TaD, in sequence of decreasing neutron yield.

The use should also be mentioned of a target consisting of a metal in which a certain amount of deuterium is accumulated as the result of deuteron bombardement. This mechanism of neutron production accounts partly for the yield of some of the solid targets listed above. This effect was already mentioned in early work of Penning and Moubis[3]).

The D_2 gas target shows a good efficiency, about five times higher than a heavy ice target. However, this would require a strongly cooled thin window, which causes an energy loss of at least 0.2 MeV, or alternatively the elaborate technique of sending a very well focussed beam through a number of small apertures, together with differential pumping.

Paraffin targets give non-monoenergetic neutrons, as a result of the competing C^{12}(d,n) N^{13} reaction. The efficiency of NaOD is about four times lower than that of heavy ice. According to our experiments with a water cooled NaOD target, the beam damages the target and removes the hydroxide.

Used at a higher temperature in the molten state the hydroxide decomposes and requires special pumping at the target. Similar objections apply to D_3PO_4. The main advantage of the zirconium target lies in its simplicity, but the short life is a serious limitation. The initial efficiency is at least five times lower than that of heavy ice; even at a relatively low specific load the yield decreases rapidly by a further factor 10 in the course of a few hours due to loss of deuterium (or tritium) and the formation of a carbonous surface film. It can be expected that the same holds for TiD and TaD targets.

3. Principle of the Rotary Ice Target

Problems envisaged are related to the relatively high vapour pressure and the low thermal conductivity of ice.

The vapour pressure at $-100°C$ is about 10^{-5} mm Hg. The low thermal conductivity makes it necessary to spread the energy to be dissipated over a larger surface. A special target has been designed, consisting of a hollow metal disc which can rotate along a vertical shaft. Between two rims near the edge of the disc an ice sheet can be frozen, forming a flat annular target. The cooling is effected by the evaporation of liquid air. The beam, by means of two sets of deflecting plates, scans an area of approximately five square centimetres.

The range of 1 MeV deuterons in ice can be computed using the molecular stopping power values of Wenzel and Whaling and is found to be 19 microns.

The advantage of the use of a rotating ice target is twofold. Firstly, the effective area is increased by a factor of about 30. The effect of the decrease of the initial heat conductivity of the ice film, as a result of lattice destruction and gas accumulation, is largely reduced. Secondly the heat capacity of the intermittently bombarded layer plays an important rôle. Furthermore, the effect of evaporation and sputtering of the ice is reduced by at least a factor 30 as compared with a stationary target.

The experience with this type of target showed that a load of 600 watt could be dissipated on a "focal spot" of five square centimetres without difficulty. The average thickness of the ice film is maintained at about 25 microns. After eight hours of operation, during which the initially

[2]) G. T. Hunter and H. T. Richards, Phys. Rev. **76** (1949) 1445.

[3]) F. M. Penning and J. H. A. Moubis, Physica **4** (1937) 1190.

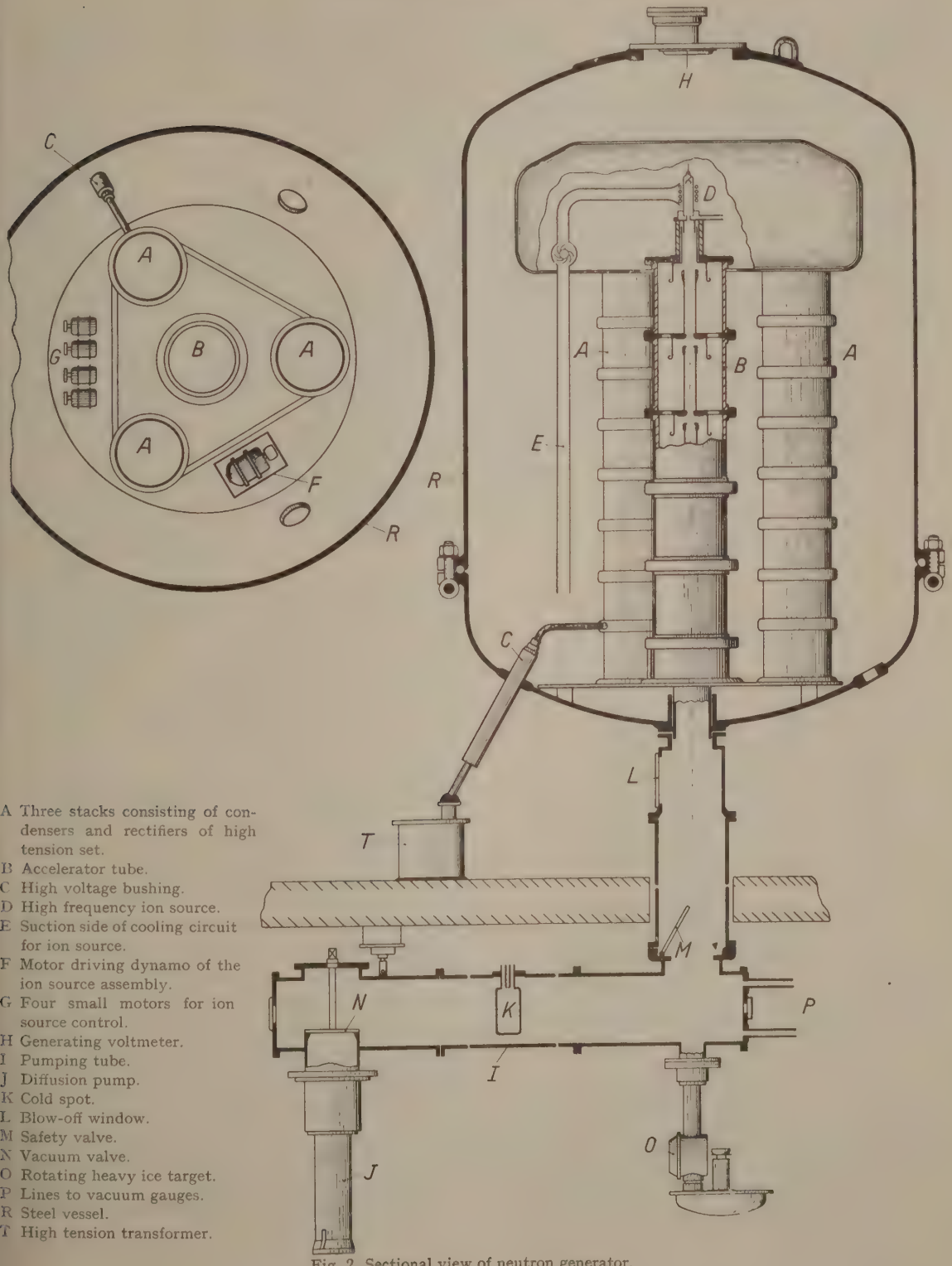

A Three stacks consisting of condensers and rectifiers of high tension set.
B Accelerator tube.
C High voltage bushing.
D High frequency ion source.
E Suction side of cooling circuit for ion source.
F Motor driving dynamo of the ion source assembly.
G Four small motors for ion source control.
H Generating voltmeter.
I Pumping tube.
J Diffusion pump.
K Cold spot.
L Blow-off window.
M Safety valve.
N Vacuum valve.
O Rotating heavy ice target.
P Lines to vacuum gauges.
R Steel vessel.
T High tension transformer.

Fig. 2. Sectional view of neutron generator.

transparent ice film has changed to a whitish opaque layer, no decrease of the neutron output could be observed, even when no fresh D_2O was supplied. The amount of D_2O necessary to prepare the target is 1 gram. The D_2O is administered by means of a vapour jet.

4. High Voltage Generator

The voltage set, together with the accelerator tube and the ion source assembly, is housed in a steel tank 10′ high and 6′8″ in diameter, suitable for a pressure of 150 lbs/sq.inch, 10 atmospheres (fig. 2).

The high voltage generator, of the cascade type (Cockcroft and Walton circuit), is built in three columns, each consisting of a number of condenser and rectifier units in identical housings mounted alternately one on top of the other.

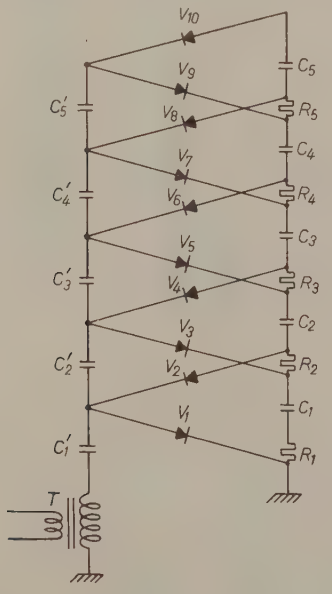

Fig. 3. Diagram of five stage cascade generator (Cockcroft and Walton) C_1, C_2, ... C_5 condensors of the "d.c." line, C_1', C_2', ... C_5' condensors of the "a.c." line, V_1, V_2, ... V_{10} selenium rectifiers, R_1, R_2, ... R_5 resistors.

There are five stages (fig. 3) and therefore there are 10 rectifiers and 10 condensers. A major advantage of the three column mounting is that the accelerator tube can stand in the centre and that a high degree of electrical symmetry is achieved.

Fig. 4 shows the construction in a schematic form. The necessary electrical connections between the condensers and the rectifiers of the

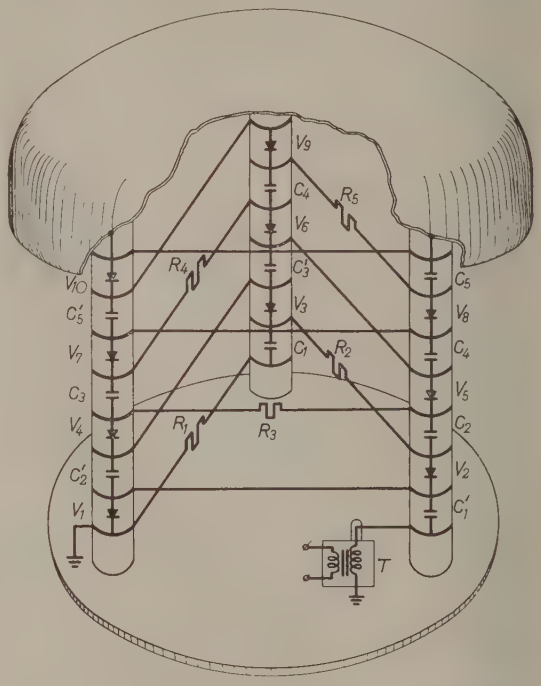

Fig. 4. Schematic view of condensors and rectifiers assembly.

different columns are made partly by means of wire-wound resistors in order to limit the maximum current in case of electrical breakdown inside the accelerator tube. The condensers have a capacity of 0.004 microfarad and are rated for 240 kilovolt.

The rectifiers are of the selenium type, rated for a reverse peak voltage of 240 kilovolt. They consist each of 9600 selenium elements mounted in series and housed in six units, each containing 1600 elements. The units are 1″ high trays, 12″ in diameter. The selenium elements are oil immersed and can carry several milliampères, without special cooling. Fig. 5 shows the mounting of the selenium rectifiers in a container.

The feeding transformer is outside the tank, the connection being made through a high voltage bushing. The transformer is rated for a maximum peak voltage of 140 kilovolt. The power is supplied by a 10 kVA 200 cycle motor-

generator. The maximum no load voltage of the high voltage set is 1200 kilovolt, the voltage drop is 100 kV/mA. The ripple voltage at no load amounts to 6 kilovolt r.m.s. and is mainly caused by capacitive voltage distribution across the rectifiers and further components of the set. The ripple increases with a further 6 kV r.m.s. per mA load.

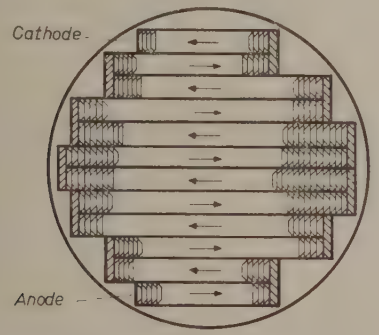

Fig. 5. Selenium rectifier unit; each rectifier V_i is composed of six units.

Special means of reducing the total ripple and voltage stabilization, are possible, but not used in the apparatus described here. The total voltage between the top corona shield and ground is measured by means of a generating voltmeter. The measuring accuracy is 1 percent.

5. Ion Source

The ion source was developed from the type described by Thonemann *et al.*[4]). The main features are high percentage of atomic ions, simplicity of construction and good life. Some of the constructional points may be mentioned here. In general a weak point in this type of ion source is formed by the glass part near the extraction electrode (probe), where puncturing not infrequently occurs. A fused silica tube, as described by Moak *et al.*[5]), proved to be very useful, especially when precision ground so as to fit closely around the probe. A further improvement was found in the use of a loose flat silica disc as the terminating part of the wall of the discharge vessel around the extractor electrode (fig. 6).

In our construction the length of the probe channel is smaller than usual and a constriction cancels the effect of reduced length on the flow of gas from the ion source tube[6]). Apparently the reduced distance between plasma and the entrance of the accelerator tube lessens the scattering losses of the extracted beam. At the same time the ion current hitting the probe was found to be smaller than with a probe of the usual form.

This reduces the number of secondary electrons travelling to the top of the tube, thus reducing the danger of puncturing of the pyrex envelope near the anode wire. This part of the ion source tube is also protected by a pyrex shield as described by Moak *et al.*

The deuterium gas is supplied through a directly heated nickel tube (length 50 cm external diameter 2.0 mm, wall thickness

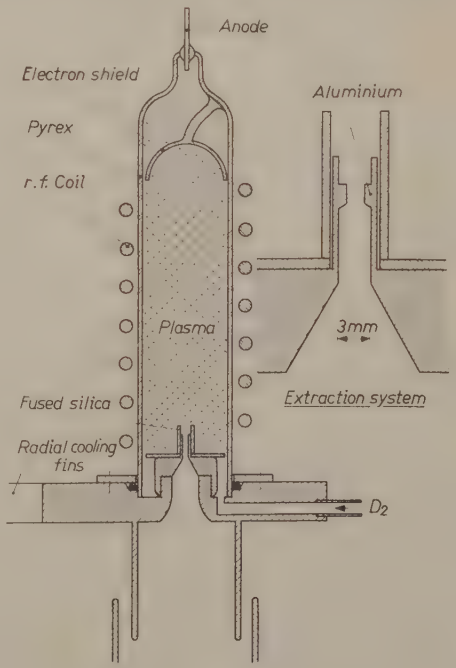

Fig. 6. High frequency ion source.

[4]) P. C. Thoneman, J. Mofatt, D. Roaf and J. H. Sanders, Proc. Phys. Soc. **61** (1948) 483.

[5]) C. D. Moak, H. Reese and W. M. Good, Nucleonics (Sept. '51) p. 18.

[6]) O. Reifenschweiler, Ann. der Physik **14** (1954) 33.

0.1 mm). This tube can withstand an internal pressure of 10 atmospheres. With a heating energy of 20 watt the temperature reaches about 400° C and the deuterium flow amounts to 20 cc/hour at atmospheric pressure. The maximum rate of flow of deuterium exceeds 50 cc/hour.

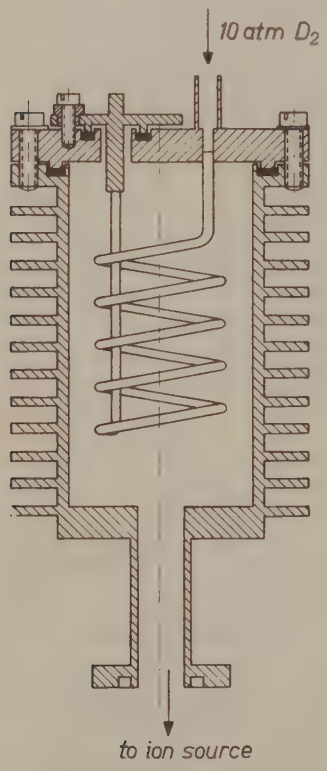

Fig. 7. Deuterium leak with directly heated coiled nickel capillary.

Several deuterium leaks of this type have been used for periods of more than 1 000 hours. Unlike palladium, nickel shows no deleterious effect of the dissolved hydrogen or deuterium and no clogging. The purity of the hydrogen obtained is very high, according to Snoek and Haes[7]). The deuterium gas is stored at a maximum pressure of 10 atmospheres in a 0.5 liter steel bottle filled with active charcoal. Filling is done by adsorbing deuterium at —180° C.

[7]) J. L. Snoek and E. J. Haes, Appl. Sci. Res. A2 (1950) 326.

The power for the ion source is supplied by a small 500 cycle 1.5 kVA alternator mounted in the top corona shield. This unit is belt-driven by a motor from the lower part of the pressure tank. In order to maintain the suitable belt tension and to avoid the transmission of vibrations to the ion source assembly, the alternator is mounted on a spring supported lever frame.

The alternator supplies the heating current for the nickel leak as well as the power for the oscillator, the rectifiers for the probe voltage (max 5 kilovolt) and the focussing voltage (max 40 kilovolt). The oscillator is a 500 Watt tuned plate—tuned grid transmitter operating at about 30 Mc. The main oscillator coil excites the discharge tube directly. Special transmitting tubes are used, specially made to operate under high external pressure.

Remote control enables the operator to supervise and regulate from the control table: deuterium flow, r.f. input, extractor and focussing voltages. The ion source tube is cooled by means of a blower which at the same time circulates the nitrogen gas in the tank. The suction side of the blower for this purpose is connected to a perspex tube extending to the lower part of the tank. The performance of the ion source can be illustrated by the following operating data: extractor voltage 2–5 kV, focussing voltage 10–15 kV, beam current at the target 0.5–1.4 mA at accelerating voltages between 300 and 1000 kV. The maximum target current depends to some extent on the accelerating potential and the degree of vacuum in the tube. The beam diameter at the target is usually smaller than 4 mm, also depending on the vacuum.

6. Accelerator Tube

The accelerator tube is composed of precision ground porcelain sections. The "spiders" supporting the drift tube are made of stainless steel, the electrodes of chrome iron. The apertures are of unequal size so as to reduce ion bombardment of the walls of the drift tubes and to stop secondary electrons. The electrodes are enveloping in order to reduce the effect of wall charges on

the beam. The vacuum seals are external O-rings of neoprene. The assembly is shown in fig. 8.

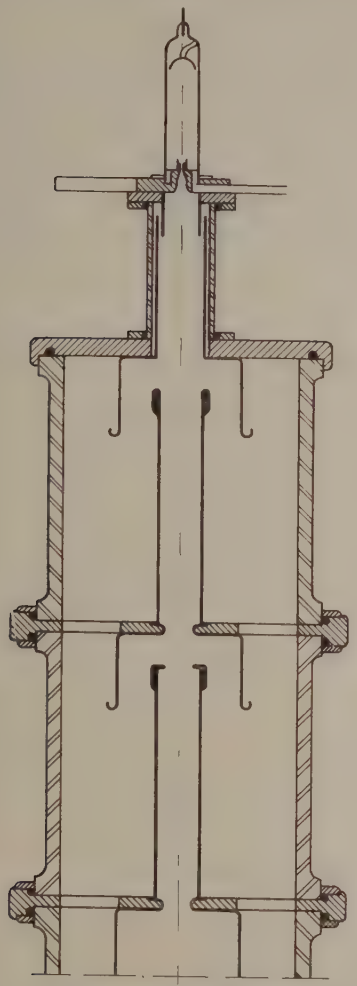

Fig. 8. Upper sections of accelerator tube with high frequency ion source.

7. Vacuum System

The vacuum system consists of a 2 000 l/sec oil diffusion pump, backed by a rotary oil pump. Provisions are made for refrigerating and a cold spot. Apart from the usual vacuum valve at the diffusion pump a special safety valve is mounted at the lower end of the accelerator tube. This valve comes into action to prevent the tank pressure from being released into the vacuum system in the event of implosion of the ion source tube or a major mechanical breakdown of one of the porcelain sections. This valve can also be operated by means of a cold cathode ionization manometer of the Penning type. Building up of any excess pressure in the vacuum system is furthermore prevented by a simple "blow off" window.

In the course of several hundreds hours of operating this safety device has not come into operation.

8. Pressure System

Though the gas used, nitrogen, is inexpensive, the transport would be an inconvenience. For this reason a steel bottle battery is used for gas storage, together with a compressor. When the tank is to be opened the gas is admitted to the compressor under atmospheric pressure, controlled by a gasometer. The vacuum produced by continuing to exhaust the tank after atmospheric pressure has been reached, facilitates the loosening or fastening of the nuts of the tank.

9. Ice Target

The construction of the rotary heavy ice target is shown in fig. 9. The beam reaches the target disc through two sets of deflector plates (only one set shown in the diagram), a cold trap and a secondary electron suppressor electrode successively.

The target disc itself, being hollow, can be cooled by the admission of liquid air through a piece of monel metal tube protruding through a slightly flexible stainless steel double walled pipe, acting as a semi floating shaft for the target drive. The shaft has enough flexibility to allow the disc to run quietly, even when some unbalance is present. Two vacuum seals are provided for, with the possibility of pumping between them. The double walled tube, acting as a Dewar vessel, avoids the danger of freezing of the rotating seals as well as waste of liquid air. The liquid air supply is controlled by a simple compressed air device. Under normal operating conditions a continuous flow of cold gas emerges from the target through a reversed chimney directed downward. The draft in this chimney

affects a hot wire anemometer at its lowest end and is indicated on the control table. The target is driven by a $\frac{1}{2}$ H.P. electric motor through a hydraulic torque converter which enables the motor to start from zero speed. The normal speed of rotation of the target is 300 rev/min.

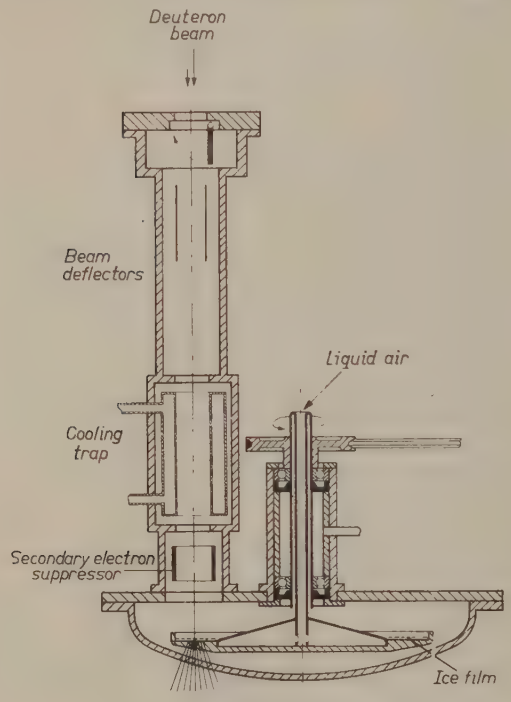

Fig. 9. Rotating heavy-ice target.

A special jet, projecting into the target housing is used for supplying heavy water vapour. The vapour pressure inside the target chamber is monitored by means of a Penning type manometer, the reading of which is a measure of the correct balance of loading and cooling of the ice target.

The target assembly is electrically insulated from earth by means of a simple O-ring.

The whole target assembly can be removed and mounted without breaking the vacuum in the accelerator tube.

10. Neutron yield Measurement

For measuring the neutron yield an ethyne (C_2H_2) filled ionization chamber was used. The type of chamber used was suggested by Dr. Munson of AERE, Harwell, England.

The wall of the chamber is composed of an electrically conducting graphite and plastic mixture, containing hydrogen and carbon atoms in equal numbers. This avoids wall corrections and makes the effective volume equal to the geometric volume. The ionization current in such a chamber, due to the neutrons produced by the bombardment of the ice target with deuterons of energy U, is expressed in ampères per ampère D_1^+ ions:

$$4\frac{pV}{l^2} L \int_0^U \frac{\sigma'(E)}{\varepsilon(E)} \frac{E_n}{2 \times 28} O(E_n)\, dE \qquad (2)$$

p = gas pressure in chamber.
V = volume of chamber.
l = average distance from target to chamber.
L = Loschmidts' number.
$\sigma'(E)$ = differential cross-section of the reaction D (d,n)He^3 for the angle concerned.
E_n = energy of neutrons produced, (in forward direction:

$$E_n = \tfrac{3}{4} Q + \tfrac{1}{2} E \left(1 + \tfrac{1}{2}\sqrt{3 + 6\, Q/E}\right)$$

Q = reaction energy = 3.28 MeV).
E = energy of bombarding deuterons at the moment of reaction
$O(E_n)$ = n–p scattering cross-section.
U = accelerating voltage.

It is assumed that the fractional average loss of energy per collision amounts to $\frac{1}{2}$, and that each ionization requires an average energy of 28 eV:

The fraction of the measured current due to gamma radiation originating by neutron capture and other secondary effects, was determined by comparison. An argon filled ionization chamber of identical size, having magnesium walls, was used for this purpose.

The relative sensitivity of both chambers for gamma radiation was found to be practically equal, as long as the same pressure was used in both chambers.

It was found that the gamma background,

measured 20 centimeters below the target in the direction of the beam was less than a few percent.

The measurements agreed within 20% with the computed value according to formula (2). A possible explanation of the difference is the formation of deposits on the wall of the ion source tube, resulting in a reduction of the atomic ion percentage of the beam. This effect is the more important, because the presence of molecular ions strongly reduces the preferential neutron intensity in forward direction, in which the measurement was made.

As a result of these negative effects on the neutron production, it was found that a beam of 300 microampères at 1 MV (or 500 microampère at 0.8 MV) was required to obtain a total flux of 10^{10} neutrons/second, whereas from a computation according to formula (2) it would follow that 250 microampère at 1 MV (420 at 0.8 MV) would be sufficient for this yield.

NUCLEAR INSTRUMENTS 1 (1957) 268–273; NORTH-HOLLAND PUBLISHING CO. – AMSTERDAM

AN A.G. CHANNEL WITH FOUR QUADRUPOLE MAGNETS

H. SCHNEIDER

Nuclear Physics Division, National Physical Research Laboratory, C.S.I.R. Pretoria

Received 15 July 1957

The known formalism of transformation matrices for the path of a charged particle in a magnetic quadrupole field is used to deduce the formulae for focus, image and object distances for a single magnet and solid angles for a system. The magnets are treated as lenses and a focussing system is constructed. From the paths in this system, conditions for the magnetic fields are found, and these conditions are shown to correspond to a simple set of equations, which are solved graphically. The usefulness of this method was checked in an experimental set-up with monochromatic electrons from an electron-gun. The caustic was measured and the working conditions were found to be in agreement with the calculations. The approximations made in calculation and experiment are discussed.

1. Introduction

Equipment for the focussing of charged particles plays an important role in the nuclear laboratory. The use of conventional magnets has the disadvantage that, even if the selection of a sharp energy band is of minor importance, transmission is relatively small. The set-up is also heavy and expensive, and can only be used for a single purpose. On the other hand, the use of quadrupoles offers interesting possibilities (as suggested by several authors[1–4]), more particularly in situations where astigmatism and dispersion are of little importance. This paper deals with the problem of focussing particles emitted in all directions from a point source.

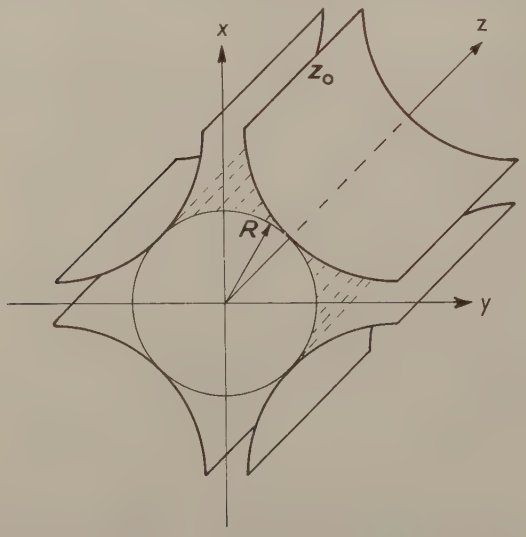

Fig. 1. The ideal quadrupole with hyperbolic polepieces and length, z_0.

2. Definitions

Let us assume an ideal quadrupole magnet with hyperbolic polepieces as indicated in fig. 1.

The magnetic potential can be described by

$$\Phi = \theta \frac{xy}{R^2}$$

where Θ is the total magnetic exitation of the quadrupole. We can then apply the linear theory of betatron oscillations. The particle may have a component of motion in the z-direction and the amplitudes in the x- and y-directions are q_x and q_y respectively.

Furthermore let

$$\left(\frac{\mathrm{d}q}{\mathrm{d}z}\right)_{xy} = q'_{xy} = p_{xy}$$

and the path of the particles is then described by the matrices:

$$M_{\text{foc}} = \begin{pmatrix} \cos \omega z & \frac{1}{\omega} \sin \omega z \\ -\omega \sin \omega z & \cos \omega z \end{pmatrix}$$

[1]) E. D. Courant, M. St. Livingston and H. S. Snyder, Phys. Rev. **88** (1952) 1190.

[2]) E. D. Courant, M. St. Livingston, H. S. Snyder and J. P. Blewet, Phys. Rev. **91** (1953) 202.

[3]) H. Friedburg and W. Paul, Naturwiss. **38** (1951) 159.

[4]) Encyclopedia of Physics *XXXIII*, Optics of Corpuscles (Springer-Verlag, Berlin, 1956).

for the focussing plane,

$$M_{\text{def}} = \begin{pmatrix} \cosh \omega z & \frac{1}{\omega} \sinh \omega z \\ \omega \sinh \omega z & \cosh \omega z \end{pmatrix}$$

for the defocussing plane,

$$M_{\text{ff}} = \begin{pmatrix} 1 & z \\ 0 & 1 \end{pmatrix}$$

for the fieldfree section, where

$$\omega^2 = c\mu_0 \frac{\theta}{R^2} \frac{1}{\sqrt{U^2 + 2U\varepsilon}},$$

ω being the oscillation number in cm^{-1}. U is the voltage corresponding to the energy of the particle and ε is its rest mass also expressed in volts. c is the velocity of light and

$$\mu_0 = 4\pi \cdot 10^{-9} \text{ vsec/A cm}$$

the permeability of the vacuum.

3. Formulae for a Single Quadrupole Magnet

If we assume that the magnet has no fringing field, we can find the focus, f, in the focussing plane (fig. 2) from

$$\begin{pmatrix} 0 \\ p_f \end{pmatrix} = (M_{\text{ff}})\,(M_{\text{foc}}) \begin{pmatrix} q_0 \\ 0 \end{pmatrix}$$

We find

$$\frac{1}{\omega \tan \omega z_0}.$$

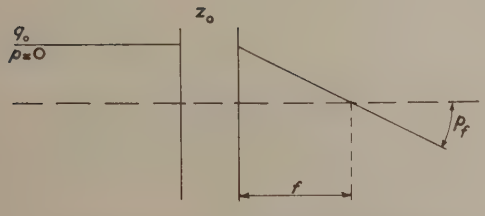

Fig. 2. The focus, f, in the focussing plane.

In the same way we find from

$$\begin{pmatrix} 0 \\ p_{f'} \end{pmatrix} = (M_{\text{ff}})\,(M_{\text{def}}) \begin{pmatrix} q_0 \\ 0 \end{pmatrix}$$

that the virtual focus, f', in the defocussing plane (fig. 3) is given by

$$f' = -\frac{1}{\omega \tanh \omega z_0}.$$

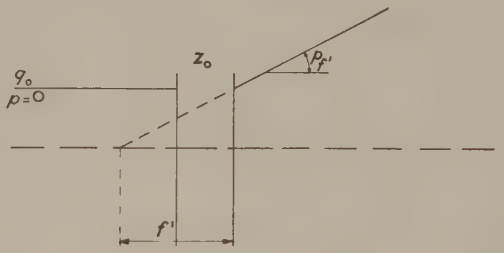

Fig. 3. The virtual focus, f', in the defocussing plane.

The components of paths in a focussing plane which come from an object on the axis at a distance s_0 from the near principal plane of the focussing system, are focussed to an image on the axis a distance s from the second principal plane (fig. 4). From the equation

$$\begin{pmatrix} 0 \\ p_1 \end{pmatrix} = \begin{pmatrix} 1 & s \\ 0 & 1 \end{pmatrix} (M_{\text{foc}}) \begin{pmatrix} 1 & s_0 \\ 0 & 1 \end{pmatrix} \begin{pmatrix} 0 \\ p_0 \end{pmatrix}$$

the distance s is

$$s = \frac{s_0 + \frac{1}{\omega} \tan \omega z_0}{s_0 \omega \tan \omega z_0 - 1}.$$

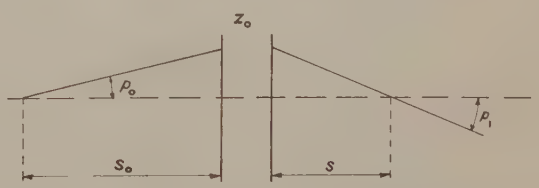

Fig. 4. Object-image-distances for the focussing plane.

In the case of the defocussing plane the equation

$$\begin{pmatrix} 0 \\ p_1 \end{pmatrix} = \begin{pmatrix} 1 & \sigma \\ 0 & 1 \end{pmatrix} (M_{\text{def}}) \begin{pmatrix} 1 & s_0 \\ 0 & 1 \end{pmatrix} \begin{pmatrix} 0 \\ p_0 \end{pmatrix}$$

gives the virtual image distance (fig. 5),

$$\sigma = -\frac{s_0 + \frac{1}{\omega} \tanh \omega z_0}{s_0 \omega \tanh \omega z_0 + 1}.$$

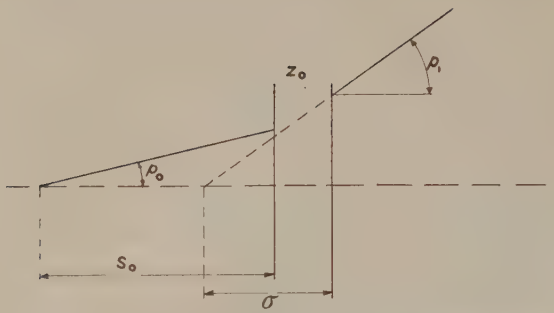

Fig. 5. Object-image-distances for the defocussing plane.

4. Construction of the Desired System

To achieve a high acceptance[5]), it is necessary to place the first magnet as near as possible to the source, and as at least two quadrupoles are needed for a collective system, the second magnet must closely follow the first. To simplify matters, the system should be symmetric, and because the total distance between object and image should not be limited by the length z_0, i.e. the distance between the two principal planes of one magnet, the symmetry plane must lie between two magnets and the total number of magnets must be even. The simplest arrangement fulfilling these demands is that with four magnets for which the paths of the particles are shown in fig. 6.

From this figure it is immediately seen that the condition

$$s\omega_I = g + |f'\omega_{II}|$$
$$f\omega_{II} = |\sigma\,\omega_I| + g$$

must be fulfilled. Addition and subtraction of these equations give

$$(s + |\sigma|)\omega_I = (|f'| + f)\omega_{II}\ ,$$
$$(s - |\sigma|)\omega_{II} = (|f'| - f)\omega_{II} + 2g\ .$$

By a suitable choice of values for z_0 and s_0 a diagram such as fig. 7 can be drawn. s_0, of course, depends on the desired transmission and on the available space (e.g. in the scattering chamber). z_0 should be of the order of R, otherwise the fringing field cannot be neglected.

The simplicity of the diagram results from the fact, that $(|f'| - f)$ is practically independent of ω for small ωz_0, so that we get horizontal lines for $(|f'| - f + 2g)$.

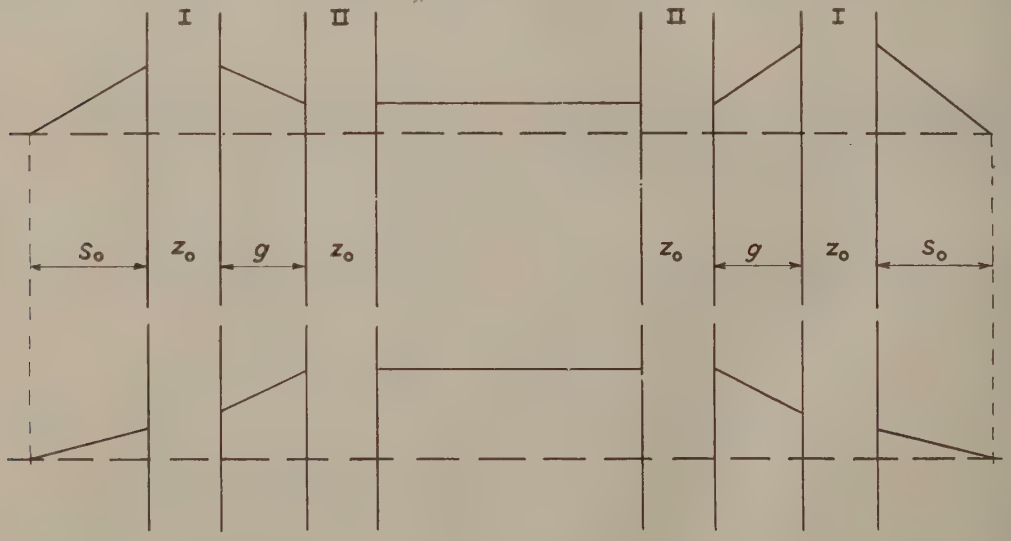

Fig. 6. The composite system for: (a) focussing plane of system 1, (b) defocussing plane of system 1.

5. Measurements with Scattered Electrons

Fig. 7 is drawn for the case of electrons and from it, we deduce that our conditions can always be fulfilled if $\omega_I \neq \omega_{II}$. With $g = 2$ cm, $\omega_I = 0.133\ \text{cm}^{-1}$ and $\omega_{II} = 0.114\ \text{cm}^{-1}$.

[5]) A. Citron and M. G. N. Hine, Suppl. Nuovo Cimento 2 (1955) 375.

With these values all geometric and magnetic values needed for an experimental arrangement are known and this has now been used to determine the effect of the approximations made. These are as follows:

(1) In the experimental arrangement, the quadrupole magnet polepieces were not hyperbolic but circular (machined on a lathe) and only 6 cm wide in the x-y-plane.

(2) The calculation has not considered the effects of fringing fields. This should result in a somewhat different z_0 which has been observed in the experiment.

(3) The finite size of the experimental source has also been neglected.

An electron-gun was mounted on a scattering chamber, so that a focussed beam of electrons hit a target of silver foil (0.2 mgr/cm²). Electrons

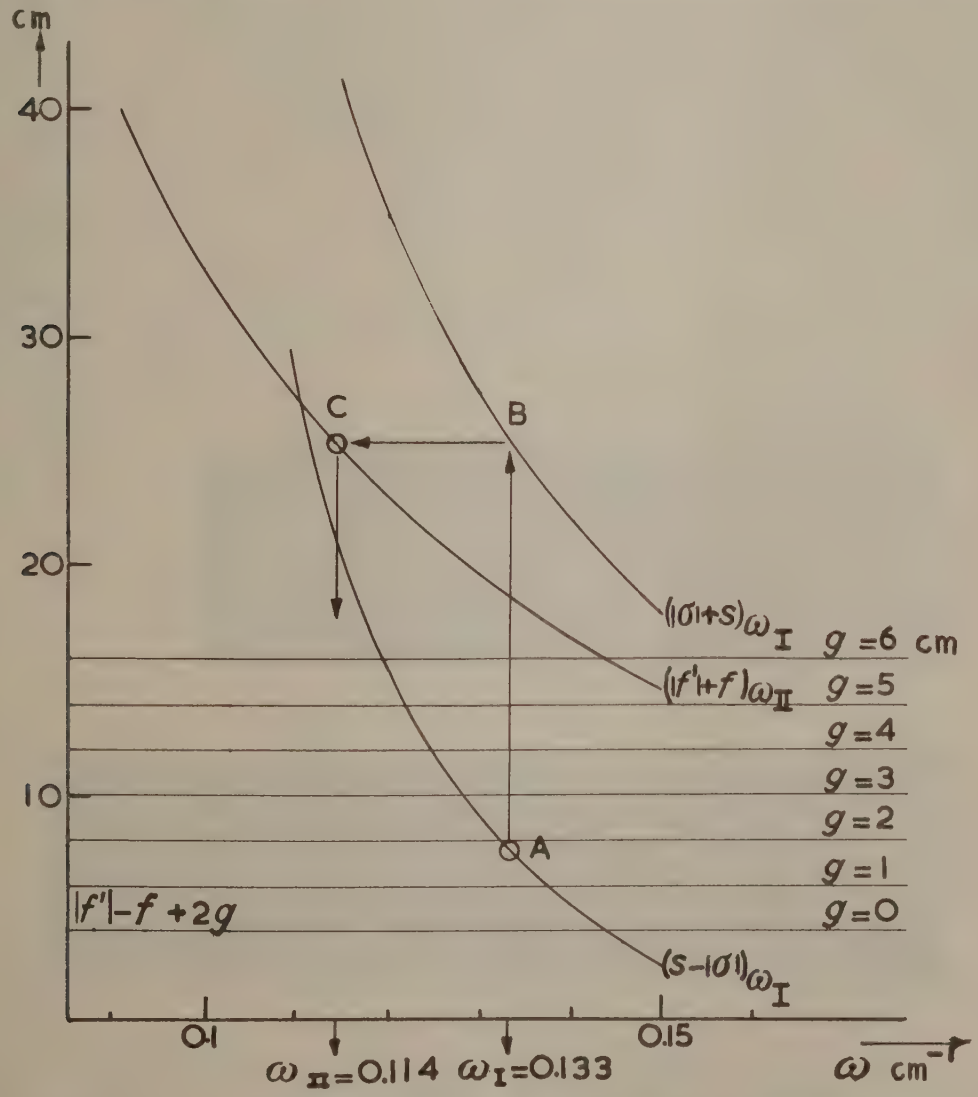

Fig. 7. Diagram showing graphical method for obtaining ω_I and ω_{II}. ω_I is given by the intersection of $(s - |\sigma|)\omega_I$ and $(|f'| - f + 2g)$ and at this value of ω_I, $(|\sigma| + s)\omega_I = (|f'| + f)\omega_{II}$. For this diagram $s_0 = 19.2$ cm and $z_0 = 6$ cm.

scattered through 90° enter a tube (6 ft long and 6″ in diameter), leading through the centre of the quadrupole magnets to a small ZnS fluorescent screen (or window counter) at its end; thus enabling observation of the focus conditions. With a magnetic flux corresponding to the focussing of 100 keV electrons, the principal planes are found to be about 1.5 cm from the end of the iron core of the magnet. The influence of the shape of the polepiece on the image was checked by the use of shims, and it was found to be not very great, due to the caustic being determined by the extreme astigmatism. Additional experimental work is being considered.

The best check of the working conditions is given by the focussing of particles of different energies. The result of such measurements are given in fig. 8.

The focus is rather sensitively dependent on the ratio ω_I/ω_{II}. The best experimental results are obtained with a value of 1.22, which taking into account the simplifying assumptions in the calculations, is in fairly good agreement with the value 1.16 from the diagram.

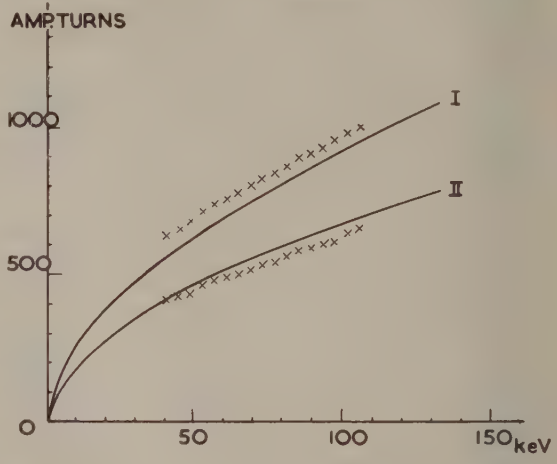

Fig. 8. The crosses indicate current in magnets I and II respectively while the system was focussing electrons of the energy given on the abscissa. The solid lines are calculated from the formula for ω, using the values for ω_I and ω_{II} obtained from fig. 7.

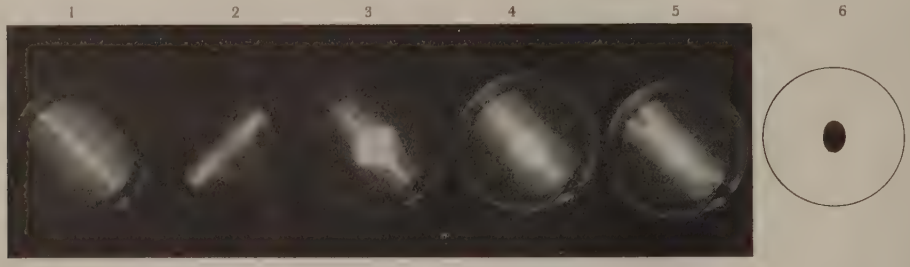

Fig. 9a.

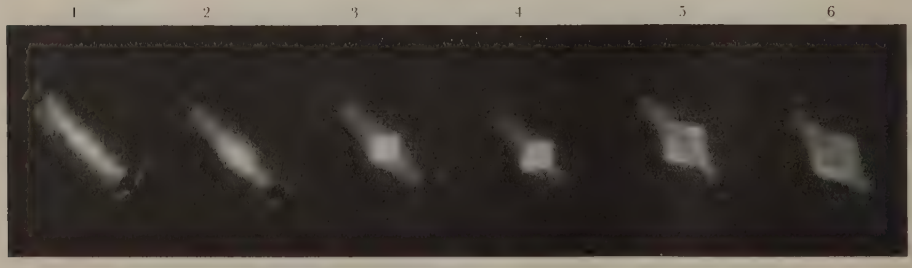

Fig. 9b.

Fig. 9. Some photographs of the focus obtained with the described system. (a) 1 shows the effect of completely defocussing one of the planes whilst focussing the other; in 2 the position is reversed. This is achieved by altering the ratio ω_I/ω_{II}. 3, 4 and 5 show the image in the near vicinity of the best focus. These were obtained by varying the total magnetic field, ω_I/ω_{II} remaining constant. 6 is a sketch of the "object" on the same scale. (b) shows the focus for 56, 60, 64, 68, 72 and 76 keV electron energy respectively, all other parameters being unchanged.

A series of photographs taken in the study of the image are shown in fig. 9.

In the first set, we see the effect of completely defocussing one of the planes whilst focussing the other. The second set shows the effect of varying the electron energy, all other conditions remaining unchanged.

6. The Transmission

The transmission depends on the maximum amplitude of the electron path. Our system has the advantage that the correspondence between the limiting values $p_{x_{max}}$ and $p_{y_{max}}$ in the source and the geometric and magnetic dimensions R, s_0, z_0 and ω, can be calculated explicitly. This is achieved as follows:

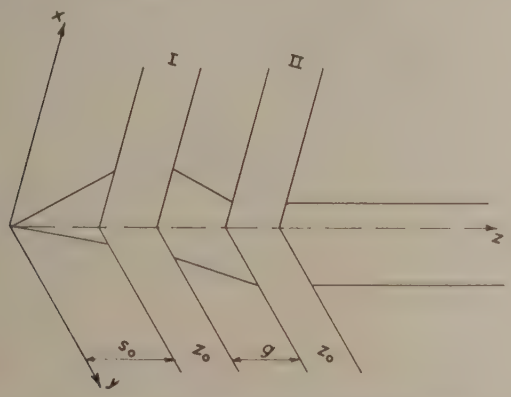

Fig. 10. Diagram illustrating the limiting conditons for $p_{x_{max}}$ and $p_{y_{max}}$.

From fig. 10, we observe that, when the first section is defocussing, the limiting path is given by

$$\begin{pmatrix} R \\ 0 \end{pmatrix} = (M_{foc})\,(M_{ff})\,(M_{def})\,(M_{ff}) \begin{pmatrix} 0 \\ p_{y\,max} \end{pmatrix}$$

and hence

$$p_{y\,max} = \frac{R\omega_{II} \sin \omega_{II} z_0}{s_0\omega_I \sinh \omega_I z_0 + \cosh \omega_I z_0} .$$

When the first section is focussing, the limiting path must be

$$\begin{pmatrix} R \\ 0 \end{pmatrix} = (M_{foc})\,(M_{ff}) \begin{pmatrix} 0 \\ p_{x\,max} \end{pmatrix} .$$

It is now necessary to calculate the z-component of the maximum amplitude (z_{max}) between the two principal planes of the first magnet. This gives:

$$z_{max} = \frac{1}{\omega_I} \tan^{-1} \frac{1}{s_0\omega_I} ,$$

and

$$p_{x\,max} = R\omega_I \sin \omega_I z_{max}$$

Of course $p_{x_{max}}$ and $p_{y_{max}}$ are different and this has great advantages in certain problems. As is known, in scattering as well as in angular correlation experiments[6]), the optimum ratio between intensity and angular resolution power requires an elliptic cross section for the detector. A rather good approximation is a rectangular form with side ratio $1/\sqrt{2}$. This holds if the variation of the angular distribution to be measured is small. In other cases the optimum ratio varies with the function to be measured[6]). Our lens-system implies a rectangular detector cross section with the side ratio of the order of $\frac{1}{2}$, and this agrees well with actual scattering experiments. The absolute value of the transmission has been checked experimentally and, even with the rough approximations mentioned above, a lower limit of 30% of the calculated value has been reached.

The loss is most probably due to these approximations and to spherical aberration.

The author would like to thank Dr. S. J. du Toit, head of the Nuclear Physics Division, for his continued interest; Mr. E. Barnard for his help in carrying out the experiments and the South African Council for Scientific and Industrial Research for permission to publish this paper.

[6]) M. Walter, O. Huber and W. Zunti, Helv. Phys. Act. 23 (1950) 697.

NUCLEAR INSTRUMENTS 1 (1957) 274–279; NORTH-HOLLAND PUBLISHING CO. – AMSTERDAM

COINCIDENCE ARRANGEMENT WITH HIGH TIME RESOLUTION USED TOGETHER WITH A 100-CHANNEL PULSE-HEIGHT ANALYZER

B. JOHANSSON

Nobel institute of Physics, Stockholm 50, Sweden

Received 17 July 1957

A time correcting circuit is described which compensates for timespread due to different pulse heights. A resolving time of $2\tau_0 = 9$ mμs is obtained with NaI(Tl) crystals for gamma energies above 50 keV.

1. Introduction

This coincidence arrangement was set up mainly for studying the decay scheme of Bi^{203} [1]) and Bi^{204} [2]). Because these two isotopes have very complicated γ-energy spectra with several weak lines it was necessary to have as good energy resolution as possible especially in the fixed channel. For that reason an intermediate image β-spectrometer of the Slätis-Siegbahn type was used in most measurements. This spectrometer gave an energy resolution of 2% at 4% transmission. The electron detector consisted of an anthracene crystal mounted on an EMI photo-multiplier.

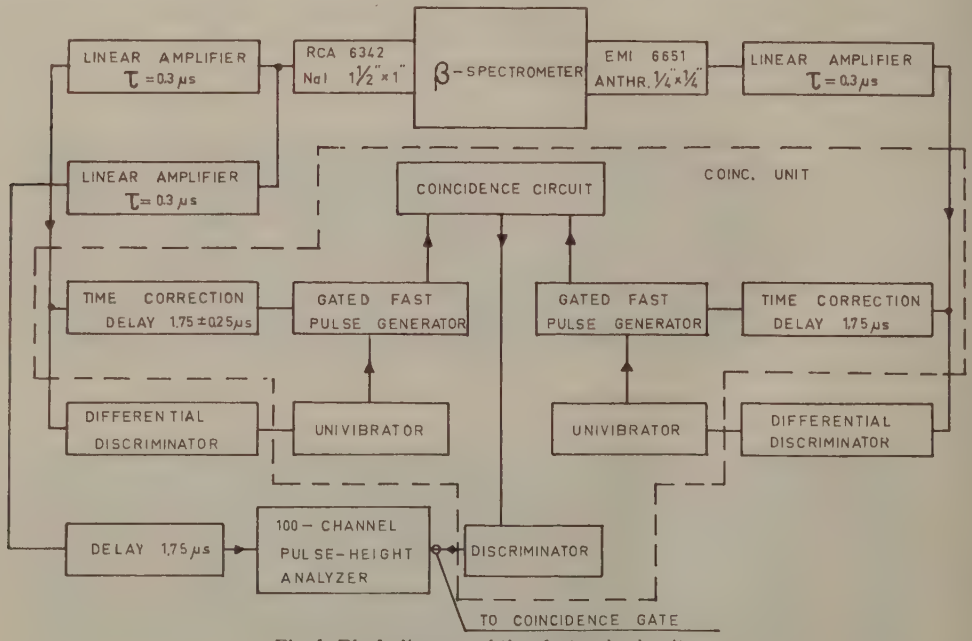

Fig. 1. Block diagram of the electronic circuits.

When a coincidence spectrum is measured one has to scan the energy range in the γ-channel in small steps. If the coincidence counting rate is low and if it is desirable to have small statistical

[1]) T. Novakov, R. Stockendal, M. Schmorak and B. Johansson, to be published in Arkiv för Fysik.

[2]) R. Stockendal, T. Novakov, B. Johansson, and M. Schmorak, to be pub ished in Arkiv för Fysik.

errors, this procedure will take very long time. In the case of short-lived isotopes it is more or less impossible to get any information about weak lines. In order to avoid these difficulties a 100-channel pulse-eight analyzer for the coindicences was used in the γ-channel.

As can be seen in fig. 1 the arrangement differs from the conventional one in that way that instead of using three coincidence circuits a gate was introduced in each channel. As has been described earlier[3]) this gate allows only pulsel with pulse heights selected by the differentias

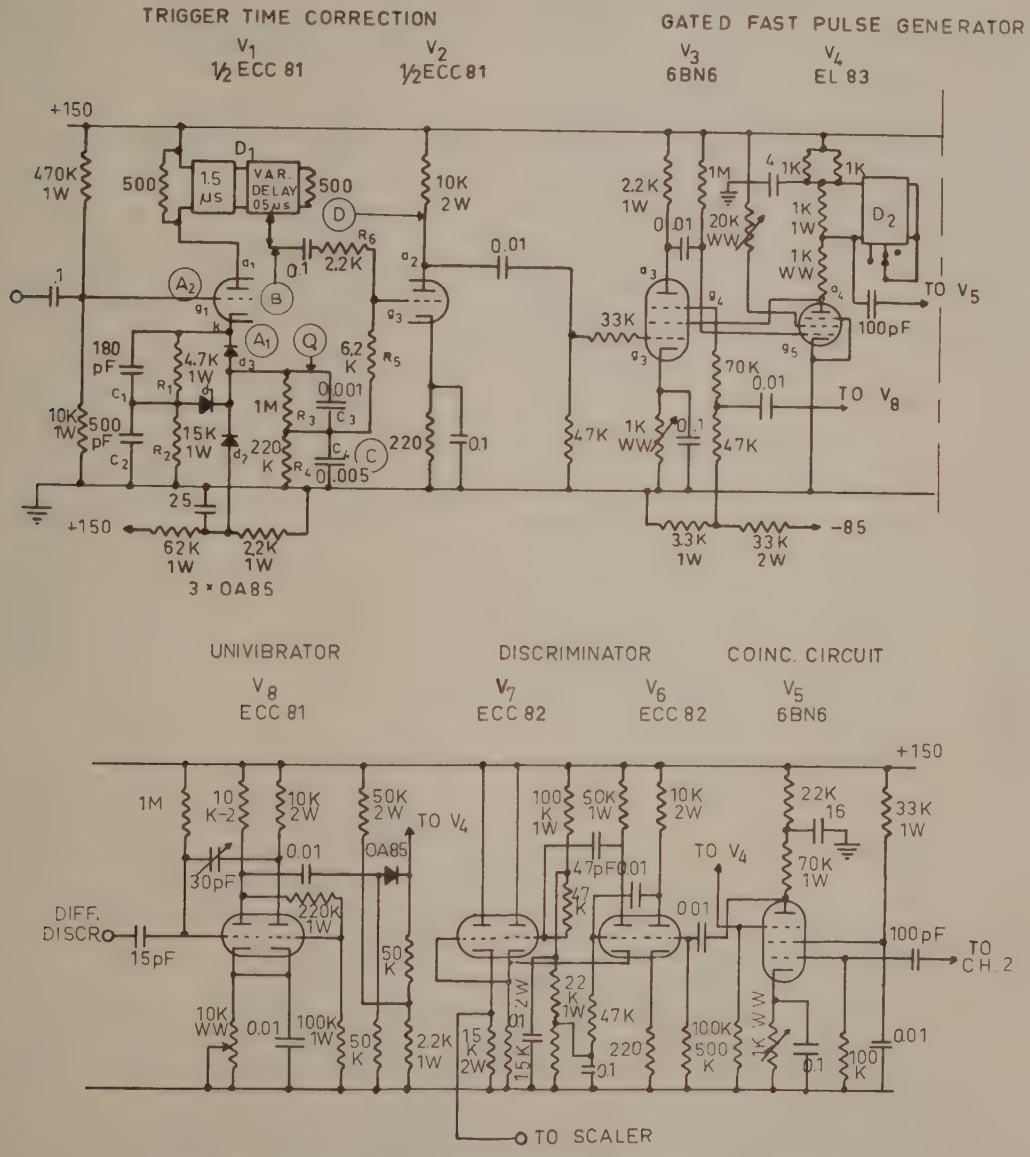

Fig. 2. Diagram of the coincidence unit. The coincidence unit is enclosed by the broken line in fig. 1.

[3]) B Åström, B. Johansson and I. Bergström, Ark. f. Fysik 12 (1957) 205.

discriminator to pass on to the coincidence circuit. The gate contains a pulse generator which fires when an incoming pulse has reached a certain triggering level and gives a fast pulse with constant rise time. Because the rise time of the detector pulses is constant a big pulse will trigger the pulse-generator earlier than a small one. To avoid this time spread a compensating unit has been designed and inserted between the linear amplifier and the gate. The linear amplifier has a gain of 2500 and gives 150 volt pulses with a rise time of 0.3 μs.

The coincidence unit consists of two equal parts, one for each channel. A complete diagram for one of these parts is given in fig. 2. The tubes V_1 and V_2 belong to the compensating circuit described later in the text. The pulse-generator consists of the two tubes V_3 and V_4. It operates as follows. If the pulse at the grid g_3 in V_3 exceeds the triggering level the anod a_3 gives a negative pulse to the grid g_5 in V_4 provided that a gate pulse has arrived at the same time at g_4. The positive pulse appearing at a_4 is then fed back to the screen grid in V_3 so that a positive feedback is obtained. This gives a fast pulse at a_4 with constant rise time. The length of this pulse is a function of the length of the trigger pulse. One tenth of the generator pulse is shortened by the delay D_2 to the proper length and fed to the coincidence tube V_5.

2. The γ-Detector

In order to increase the energy resolution of the γ-detector a special arrangement was used. The spectrometer used had a 15 cm thick pole-piece in each end. The sample was mounted inside the spectrometer in front of one of these pole pieces, and because it was important to have a large solid angle for the γ-detector the crystal had to be placed close to the sample.

It was found that a light-guide of 15 cm length gave only half as good energy resolution as was obtained without a light-guide. For this reason the crystal was mounted directly on the multiplier. But with the detector placed inside the pole piece the influence of the stray magnetic field on the multiplier reduced the energy resolution in proportion to the current through the spectrometer. In order to avoid this influence a coil was wound around the cover of the multiplier. The arrangement is shown in fig. 3. With a proper current through this coil the pulse height of the multiplier pulses could be increased to

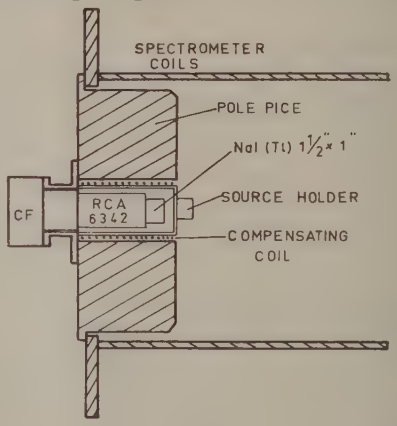

Fig. 3. The compensating coil arrangement of the β-spectrometer.

95% of the pulse height without field. In this way an energy resolution of 9.5% was obtained for the 662 keV γ-ray of Cs^{139} with a current through the spectrometer corresponding to the focusing of 1 MeV electrons.

3. The Time Correcting Unit

As mentioned above a big pulse will trigger the pulse generator earlier than a small one. This gives rise to a time spread and reduces the optimal resolving time especially when a large pulse height range is investigated at the same time as is the case when a multichannel analyzer is used.

This time spread can be compensated for in the following way. If one assumes that the pulses have triangular shape and constant rise time a simple geometrical reasoning shows how much the base line of a pulse shall be lowered if its leading edge shall pass through a certain point. If the pulse V in fig. 4 A shall pass through the point P, determined by the amplitude V_0 and the trigger level V its bias shall be lowered to the level

$$-\left(\frac{\Delta V}{V_0}V-\Delta V\right).$$

This is illustrated in fig. 4 B. Fig. 5 shows how this subtracting is carried out in the compensating circuit. The figures are not drawn in the right proportions. The incoming pulse A is delayed 1.75 μs (B) in order to appear at the flat

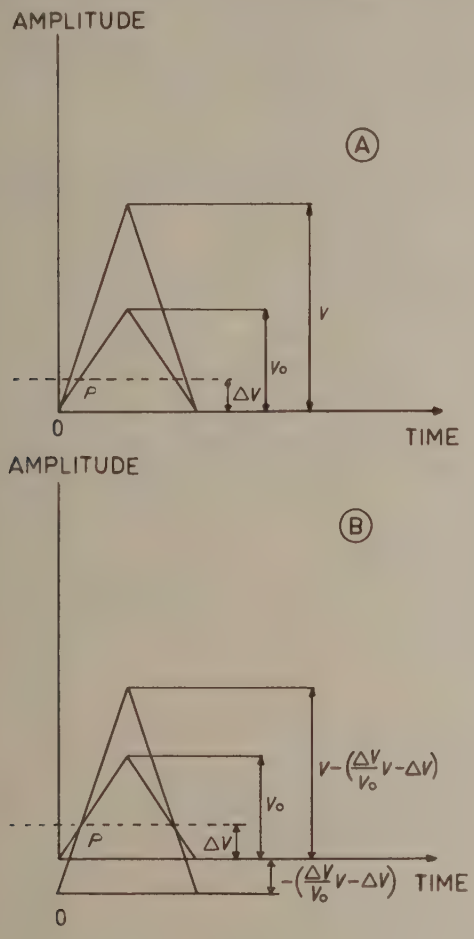

Fig. 4

top of C to which it is added. Another reason for the delay of 1.75 μs is to compensate for delay in the discriminators. The pulse C is produced in a subtracting and lengthening circuit and has the amplitude $((\Delta V/V_0)V - \Delta V)$. The result of this adding is shown in fig. 5 D. The compensating circuit operates in the following way. A positive pulse is fed to the input I (fig. 2). The tube V_1 inverts the phase and has a gain of 0.1. The negative pulse appearing at a_1 is sent via the delay D_1 to the grid g_2 of the tube V_2 where it is amplified 10 times. The ratio of amplification in the circuit is thus 1:1. The pulse that has to be subtracted from the delayed one is produced in the catode circuit of V_1 and is sent to the grid g_2 via R_5.

The cathode pulse of V_1 is divided in the ratio $\Delta V/V_0$ by the resistances R_1 and R_2 and the capacitances C_1 and C_2. When the voltage on R_2, C_2 exceeds the voltage level ΔV in the point Q the diode d_1 becomes conducting and the condensor $C_3 + C_4$ is charged to the value $((\Delta V/V_0)V - \Delta V)$. The voltage level ΔV is maintained by the diode d_2. Because of the large time constant $(C_3 + C_4) \times (R_3 + R_4)$ the voltage on

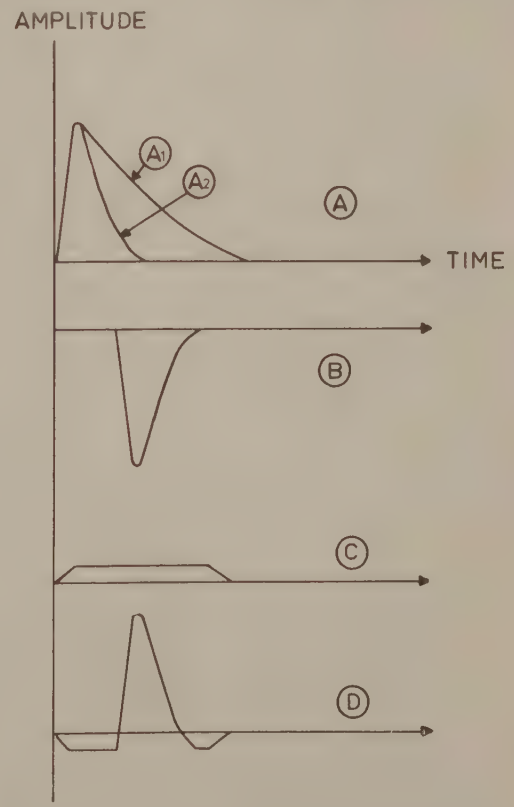

Fig. 5. Pulse shapes in the correction circuit. The letters A, B, C and D refer to pulse chapes at different points of fig. 2.

$C_3 + C_4$ is constant until the cathode pulse at k disappeares when $C_3 + C_4$ is discharged through the diode d_3. The pulse shape is shown

in fig. 5 C. This pulse is then added to the delayed pulse in the grid circuit of V_2 and the pulse appearing at the anode a_2 is that shown in fig. 5 D.

From the decay time of the scintillation flash in a NaI(Tl)-crystal and the time constant of the anode circuit of the photomultiplier it is easy to determine the pulse shape. The increase in V in the time dt is

$$dV = (\lambda_1 K \cdot e^{-\lambda_1 t} - \lambda_2 V)dt$$

where V = the amplitude of the multiplier pulse

λ_1 = decay constant of the scintillation material

K = constant proportional to the amount of photo electrons from each scintillation

λ_2 = time constant of the anode circuit of the multiplier

If $\lambda_1 = \lambda_2$ the solution is

$$V = K \cdot \lambda_1 t \cdot e^{-\lambda_1 t}$$

with the maximum at $t = 1/\lambda_1$.

The rise time is thus constant. For a certain time t_P corresponding to the point P in fig. 5 the pulse height is

$$V_P = K \cdot \lambda_1 t_P \, e^{-\lambda_1 t_P}$$

This is a linear function of K as well as $V_{max.}$ is a linear function of K so that the ratio $V_P/V_{max.}$ = constant. The conditions required in the compensating circuit are thus satisfied. The restriction that the pulses should have triangular shape is not necessary provided that the conditions above are satisfied.

To test the performance of the apparatus three measurements were made with a different resolving time in each case. The result is shown in fig. 7. The sample used was Bi^{207}, which has two strong γ-lines in coincidence. The upper curve of fig. 6 shows the γ-spectrum for Bi^{207}, and below this is the coincidence spectrum drawn for coincidences with the 1064 keV line. The resolving time was 9 mμs in this case. The three curves of fig. 7, show the same coincidence spectrum taken with three different resolving times. As can be seen the counting rate is the same throughout the curves in all the three cases. The efficiency is thus constant and nearly

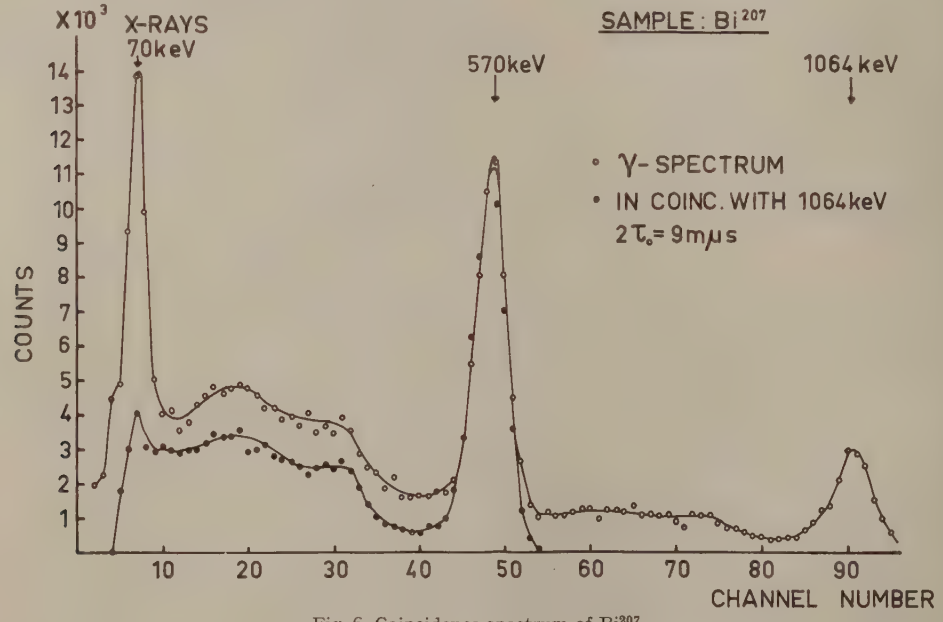

Fig. 6. Coincidence spectrum of Bi^{207}

100% even for the smallest resolving time. $2\tau_0 = 9$ mμs seems to be the limit for low energy γ-rays because the efficiency begins to drop at 70 keV if the resolving time is decreased. When the above measurements were made the apparatus was arranged for γ-γ coincidence measurements.

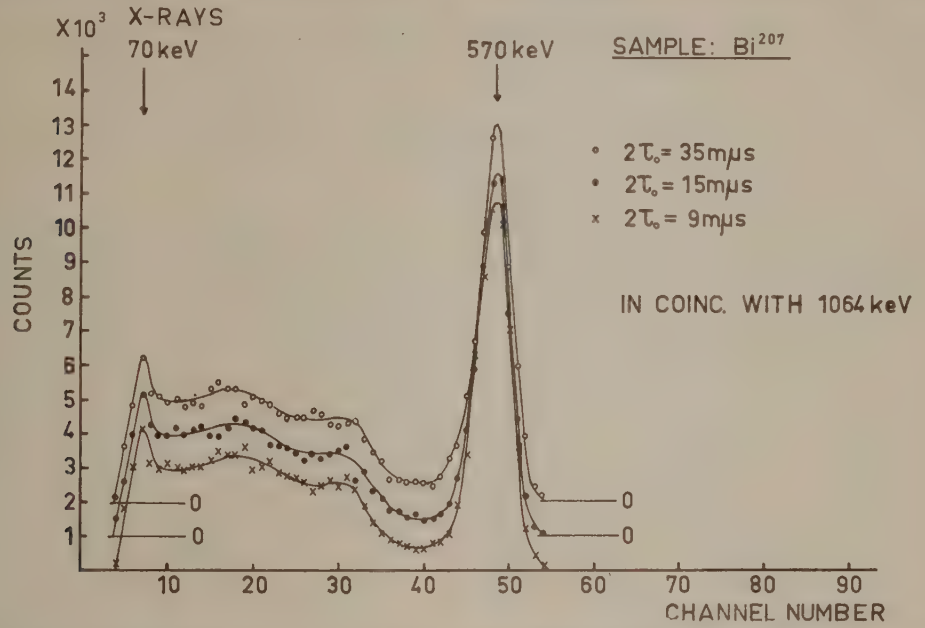

Fig. 7. The same coincidence spectrum as in fig. 6 taken at three different resolving times. Because the three curves are almost identical they have been displaced in the y-direction. A 1 mm thick cadmium absorber is used to decrease the X-ray intensity.

NUCLEAR INSTRUMENTS 1 (1957) 280–281; NORTH-HOLLAND PUBLISHING CO. – AMSTERDAM

LETTER TO THE EDITOR

A NEW PARTICLE ACCELERATOR

YATENDRA PAL VARSHNI

Department of Physics, Allahabad University, Allahabad

Received 5 February 1957

Within a few years of the construction of the first Cyclotron, it was realized[1]) that it will not be possible to accelerate ions by means of the Cyclotron beyond a certain limit on account of the relativistic increase in mass of the accelerated particles at high velocities and the consequent departure from resonance. Bethe and Rose[1]) suggested to partly remedy the situation by increasing the peak value of the accelerating potential, thus reducing the number of revolutions needed to reach a particular radius. This was utilized in the construction of the University of California 60 in. cyclotron[2]).

In 1945 McMillan[3]) and Veksler[4]) proposed to overcome this difficulty by varying the frequency of the accelerating potential and/or the magnetic field (for earlier history of the proposal see Mann[5]). Based on these were built Synchrocyclotron[6]) (frequency modulation), Electron Synchrotron[7,8]) (variation of magnetic field) and Proton Synchrotron[9–12]) (frequency modulation as well as variation of the magnetic field). In recent years interest is growing on Alternate Gradient Focusing[12–14]).

The present note suggests a new method that overcomes the relativistic limitation by changing the shape of the dees.

The essential principle can be explained as follows (see fig. 1):

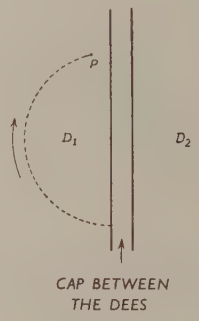

Fig. 1

Consider the motion of a particle, in a cyclotron, having energy in a region where relativistic effects become important, and is just getting out of phase with the accelerating potential on the other dee D_2. Let its position in such a situation be P (the effect has been exaggerated in the diagram). Then it is obvious that if it had not to traverse the remaining distance in the dee D_1 it would have been accelerated in the right

[1]) H. A. Bethe and M. E. Rose, Phys. Rev. **52** (1937) 1254.

[2]) E. O. Lawrence, L. Alvarez, W. Brobeck, D. Cooksey, D. Corson, E. McMillan, W. Salisbury and R. Thornton, Phys. Rev. **56** (1939) 124.

[3]) E. M. McMillan, Phys. Rev. **68** (1945) 143; ibid. **69** (1946) 534.

[4]) V. I. Veksler, J. Phys. U.S.S.R. **9** (1945) 153; Phys. Rev. **69** (1946) 244.

[5]) W. B. Mann, The Cyclotron, (Metheun and Co. Ltd., 1953).

[6]) W. M. Brobeck, E. O. Lawrence, K. R. Mackenzie, E. M. McMillan, R. Serber, D. C. Sewell, K. M. Simpson and R. L. Thornton, Phys. Rev. **71** (1947) 449.

[7]) F. K. Goward and D. E. Barnes, Nature **158** (1946) 413.

[8]) H. C. Pollock, Phys. Rev. **69** (1946) 125; F. R. Elder, A. M. Gurewitsch, R. V. Langmuir and H. C. Pollock, J. Appl. Phys. **18** (1947) 810.

[9]) M. S. Livingston, Phys. Rev. **73** (1948) 1258(A).

[10]) M. S. Livingston, J. P. Blewett, K. Green and L. J. Haworth, Rev. Sci. Instr. **21** (1949) 7.

[11]) Cosmotron Staff, Rev. Sci. Instr. **24** (1953) 723.

[12]) M. S. Livinston, High Energy Accelerators (Interscience Publishers, New York, 1954).

[13]) E. Courant, M. S. Livingston and H. Snyder, Phys. Rev. **88** (1952) 1190.

[14]) N. Christofilos, Focusing system for Ions and Electrons and Application in Magnetic Resonance Particle Accelerators (Privately printed report, 1950).

phase. This can be achieved by changing the shape of the dees. The proposed shape is shown

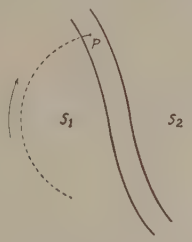

Fig. 2

in fig. 2. With such a shape of the dees, the particle will be further accelerated in the right phase. During its motion in S_2 there will be a further lag which is compensated in a similar manner by S_1, and so on. Thus the particle will always arrive in the gap between the dees after exactly equal time intervals. Ultimately the dees will be spiral shaped as shown in fig. 3 (only $1\frac{1}{2}$ revolutions of the spirals have been shown; there may be many more). It may be noted that the dees spiral in the direction opposite to the direction of motion of the particle.

Let

$E_0 = m_0c^2$ rest energy of the particle
T = Kinetic energy
e = Charge of the particle
B = Magnetic field
r = Radius of the path of the particle,

then the angle ϕ made by the particle inside a dee after each acceleration is given by

$$\phi = \frac{\pi}{1 + T/E_0} \tag{1}$$

and the radius r is determined by the equation

$$T^2 + 2TE_0 = c^2e^2B^2r^2. \tag{2}$$

Knowing ϕ and r from equations (1) and (2), the exact shape of the spiral dees can be calculated.

This accelerator will have the advantage that unlike Synchrocyclotron and Synchrotron which have a low average ion output (about 1 % of the conventional cyclotron[12]), it will give the average output of the same order as a cyclotron. However, like Synchrocyclotron it will also require a solid core magnet, and likewise the difficulties associated with gigantic magnets may limit the maximum energy possible. Later on it may be possible to build an accelerator incorporating all the three viz. frequency modulation, variation of magnetic field and spiral dees.

The suggested accelerator may be called the "Spiratron" (short form of Spiralotron).

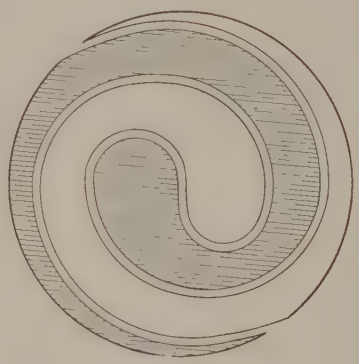

Fig. 3

The facing edges of Spiratron dees would be parallel, and the lines of force would be perpendicular to the two edges. Still the slanting nature of the edges may lead to greater radial oscillations of the particle than in the case of cyclotron. This can be countered by using radially decreasing field:

$$B = B_0(r_0/r)^n \tag{3}$$

where n is less than 1. Equation (2) would be accordingly modified. Such a field provides good restoring forces for radial displacements. A high dees voltage would also be helpful in minimising radial oscillations. The details of the focusing conditions are being studied.

The author is thankful to Prof. K. Banerjee for his kind interest in the work.

NUCLEAR INSTRUMENTS 1 (1957) 282–288; NORTH-HOLLAND PUBLISHING CO. – AMSTERDAM

RÉDUCTION DES DISPERSIONS DANS LES DÉTECTEURS À SCINTILLATION

J. F. VERVIER et P. C. MACQ

Centre de Physique Nucléaire de l'Université de Louvain, Louvain (Belgique)

Received 16 July 1957

The influence of resistance R and capacity C between the anode of the photomultiplier and mass, on time dispersion of pulses from a scintillation detector due to amplitude fluctuations, has been studied. Optimum conditions for minimizing that dispersion are discussed. Some experimental arrangements for reducing capacity C, and so time dispersion, are described.

1. Introduction

Les impulsions qui apparaissent à l'anode des photomultiplicateurs, dans les compteurs à scintillation, subissent deux sortes de fluctuations: leur amplitude varie autour d'une valeur moyenne, fonction de la nature et de l'énergie de la particule détectée; il y a d'autre part une dispersion dans l'intervalle de temps entre le passage de la particule dans le cristal et l'arrivée de l'impulsion à l'anode des photomultiplicateurs. Ces deux fluctuations ne sont d'ailleurs pas indépendantes: comme l'ont montré divers auteurs (réf.[1])) et comme nous le verrons dans la suite, une dispersion en amplitude provoque une dispersion dans le temps, lorsqu'on fait passer les impulsions dans des circuits de coincidences rapides.

Les principales causes de dispersion en amplitude sont les suivantes (réf.[1–3])):

(1) fluctuation dans le nombre de photons produits dans le cristal, par une particule de nature et d'énergie donnée.

(2) fluctuation dans la transmission de ces photons à travers le cristal et le guide de lumière, jusqu'à la photocathode.

(3) fluctuation dans le nombre d'électrons produits par ces photons à la photocathode et dans la collection de ces photoélectrons sur la 1° dynode.

(4) fluctuation dans la multiplication des électrons dans le photomultiplicateur.

En admettant une distribution de Poisson comme résultante des trois premiers types de fluctuations, et en utilisant les calculs de Morton (réf. [4])) et de Wright (réf. [5])) pour le quatrième type, on obtient les expressions suivantes pour la forme de l'impulsion à la sortie du photomultiplicateur, $V(t)$, et sa variance, $\sigma^2(t)$ (réf. [6]) et [7])):

$$V(t) = \frac{\bar{Q}_0}{C} \frac{RC}{\tau - RC} \left[e^{-t/\tau} - e^{-t/RC} \right], \qquad (1)$$

$$\sigma^2(t) = \left(\frac{\bar{Q}_0}{C}\right)^2 \frac{\bar{s}}{\bar{s}-1} \frac{1}{\bar{n}p} \frac{RC}{2\tau - RC} \left[e^{-t/\tau} - e^{-2t/RC} \right], \qquad (2)$$

$$\bar{Q}_0 = e\bar{n}p\bar{s}^{r},$$

e est la charge de l'électron; n est le nombre de photons qui arrivent à la photocathode; $\bar{n}$ sa moyenne; p est la probabilité pour qu'un photon produise, à la photocathode, un électron qui soit recueilli par la 1° dynode; $\bar{s}$ est la multiplication moyenne par étage du photomultiplicateur, et r, le nombre d'étages; R est la résistance et C la capacité entre l'anode du photomultiplicateur

[1]) E. Baldinger et W. Franzen, Amplitude and Time Measurements in Nuclear Physics (Advances in Electronics and Electron Physics, Éditeur L. Marton. Vol. VIII, 1956).

[2]) E. Breitenberger, Scintillation Spectrometer Statistics (Progress in Nuclear Physics, Éditeur O. Frisch, Vol. 4, 1955).

[3]) A. Meessen, Étude des rayons γ par les compteurs à scintillation (Mémoire de licence, Louvain, 1955).

[4]) G. A. Morton et J. A. Mitchell, R.C.A. Review 9 (1948) 632.

[5]) G. T. Wright, Journal of Scient. Instr. 31 (1954) 377.

[6]) A. Lundby, Archiv for Math. og Naturv. B L1 (1952) 91.

[7]) G. T. Wright, Proc. Phys. Soc. B LXIX (1956) 358.

et la masse; τ est le temps de décroissance du cristal.

L'impulsion atteint son maximum pour un temps

$$t'_m = \frac{\tau RC}{\tau - RC} \ln \frac{\tau}{RC} \qquad (3)$$

et sa pente à l'origine vaut

$$\left(\frac{dV}{dt}\right)_{t=0} = \frac{\bar{Q}_0}{C\tau} \qquad (4)$$

Les principales causes de dispersion dans le temps sont les suivantes (réf. [1]) et [8])):

(1) fluctuation dans le temps d'émission des photons par le cristal, due au temps de décroissance fini du cristal.

(2) fluctuation dans le temps de passage des photons du cristal à la photocathode, par suite des différences de parcours dans le cristal et le guide de lumière.

(3) fluctuation dans le temps de transit des électrons entre la photocathode et l'anode, à cause des variations des trajectoires.

Ces trois types de fluctuations, donc aussi leur résultante, sont approximativement régis par la loi de Poisson; les dispersions sont de 10^{-9} sec environ pour le guide de lumière (réf. [9])) et de l'ordre de 2×10^{-9} sec pour le photomultiplicateur (réf. [1]) et [8])).

L'influence de la dispersion en amplitude sur la dispersion dans le temps a été étudiée en détails par divers auteurs (réf. [10])), notamment par Baldinger et Franzen (réf. [1])); ceux-ci ont tenu compte du temps de décroissance fini du cristal, ainsi que des fluctuations dans la transmission des photons à la photocathode et dans leur conversion en photoélectrons. Nous donnons dans le paragraphe 1, une méthode graphique permettant d'étudier qualitativement cette influence, méthode équivalente aux calculs plus précis de Baldinger et Franzen. Nous avons d'autre part étudié l'influence des constantes R et C sur la dispersion en amplitude, et nous donnons au paragraphe 2 quelques dispositifs expérimentaux susceptibles de diminuer cette dispersion. Nous signalons également une méthode graphique permettant de combiner les dispersions dans le temps introduites par le guide de lumière et le photomultiplicateur, avec les dispersions produites par les fluctuations en amplitude.

[8]) P. Macq, Étude de la corrélation angulaire β-γ (Thèse de doctorat, Louvain, 1955).

[9]) A. Lundby, Rev. Scient. Instr. **22** (1951) 324.

[10]) R. F. Post et L. I. Schiff, Phys. Rev. **80** (1952) 1113.

2. Dispersion dans le temps des Impulsions

2.1. FORME ET VARIATIONS EN AMPLITUDE DES IMPULSIONS

Nous avons calculé la forme de l'impulsion à l'anode du photomultiplicateur, $V(t)$, et sa variance $\sigma^2(t)$ pour différentes valeurs de τ/RC, d'après les équations (1) et (2); supposant C constant, nous choisissons $\bar{Q}_0/C = 1$, $\bar{s} = 4$ et $\bar{n}\bar{p} = 100$. La figure 1 donne la forme des impulsions pour 5 valeurs de τ/RC: 100, 10, 1, 1/10, 1/100; le temps est exprimé en unités de τ.

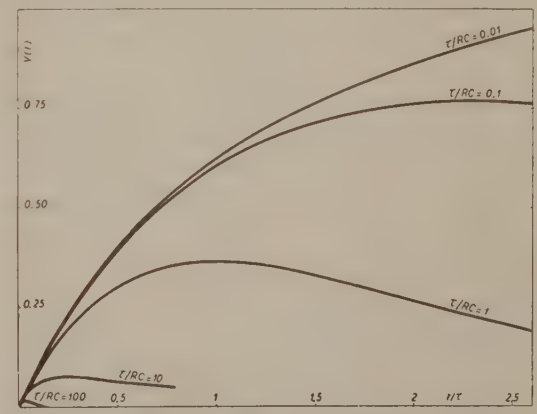

Fig. 1. Forme des impulsions à l'anode des photomultiplicateurs pour 5 valeurs de τ/RC. On suppose C constant. Le temps est exprimé en unités de τ.

La pente à l'origine est la même pour toutes les courbes, car on a supposé C constant (éq. (4)); par contre, le temps du maximum t'_m, et la hauteur de l'impulsion à ce maximum augmentent rapidement avec RC/τ. Des courbes de ce genre ont déjà été tracées par Lundby (réf. [6])). Les figures 2 à 4 représentent les courbes de $V(t) \pm \sigma(t)$ en fonction de t/τ, avec des échelles différentes pour les diverses valeurs de τ/RC. La forme de l'impulsion est la même, au changement d'échelle près, pour deux valeurs inverses

de τ/RC, mais les variations relatives sont beaucoup plus faibles pour RC/τ grand.

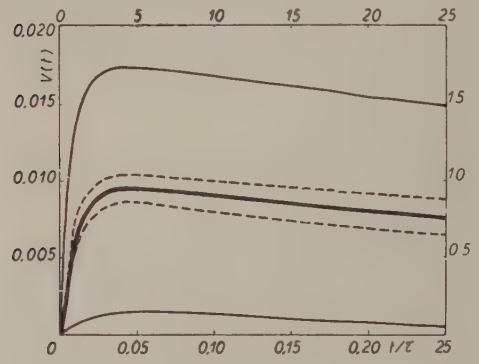

Fig. 2. Forme et variations des impulsions pour deux valeurs inverses de τ/RC: 100 (échelle en bas et à gauche; trait plein fin) et 1/100 (échelle en haut et à droite; trait interrompu). La forme de l'impulsion (trait plein épais) est la même, au changement d'échelle près, pour les deux valeurs de τ/RC.

Les circuits de coincidences rapides (réf. [1]) sont basés sur une addition non linéaire des 2 impulsions dont on étudie les coincidences; la "somme" ainsi obtenue (fig. 5) passe dans un discriminateur dont le seuil détermine d'ailleurs

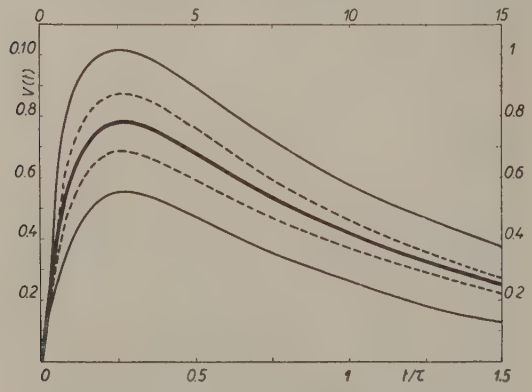

Fig. 3. Forme et variations des impulsions pour deux valeurs inverses de τ/RC: 10 (échelle en bas et à gauche; trait plein fin) et 1/10 (échelle en haut et à droite; trait interrompu).

le temps de résolution. On voit, sur les fig. 2 à 4, que, par ce procédé, une variation dans l'amplitude de l'impulsion entraine une incertitude sur le temps t_1 où l'impulsion passe le seuil du discriminateur; par exemple pour $\tau/RC = 1$ (fig. 4, courbe a), si le seuil correspond à $V = 0.2$, t_1 est compris entre $0.18\,\tau$ et $0.36\,\tau$, valeurs obtenues en coupant, par la droite $V = 0.2$, les courbes de l'amplitude de l'impulsion et de ses variations. Cette méthode graphique permet d'étudier qualitativement la disper-

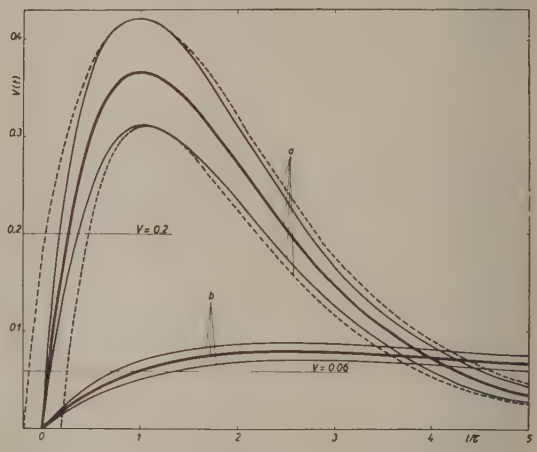

Fig. 4. Courbes a: Forme (trait plein épais) et variations (trait plein fin) des impulsions pour $\tau/RC = 1$; les courbes en traits interrompus représentent la dispersion totale dans le temps obtenue en combinant la dispersion due aux fluctuations en amplitude et celle introduite par le guide de lumière et le photomultiplicateur, par la méthode exposée au paragraphe 2. Courbes b: forme (trait plein épais) et variations (trait plein fin) des impulsions pour une capacité C dix fois plus grande que pour la courbe a, mais la même résistance R et le même temps de décroissance τ.

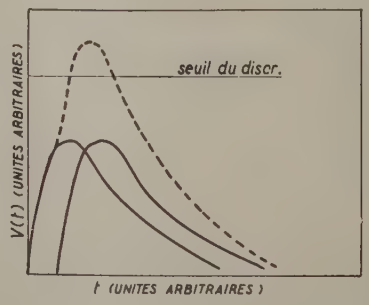

Fig. 5. Addition non linéaire de 2 impulsions (trait plein) dans les circuits de coincidences rapides. La "somme" (trait interrompu) passe dans un discriminateur dont le seuil détermine le temps de résolution.

sion dans le temps produite par les fluctuations en amplitude pour une valeur donnée du seuil du discriminateur; elle est équivalente à la

méthode analytique de Baldinger et Franzen (réf. [1])). Pour réduire cette incertitude sur le temps, il faut diminuer les variations relatives dans la hauteur de l'impulsion, en choisissant une constante RC appropriée.

A l'entrée des circuits de coincidences rapides, on réduit souvent la durée de l'impulsion en la coupant au moyen d'un cable coaxial court-circuité à une de ses extrémités qui réfléchit l'impulsion en changeant son signe (fig. 6). Par

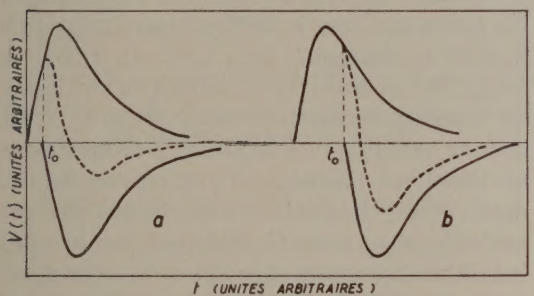

Fig. 6. Réduction de la durée d'une impulsion par coupure au moyen d'un cable coaxial court-circuité à une de ses extrémités qui réfléchit l'impulsion en changeant son signe; l'impulsion résultante est dessinée en traits interrompus. Pour la courbe a, le temps de coupure se situe avant le temps du maximum de l'impulsion; pour la courbe b, il se situe après.

ce procédé, le maximum de l'impulsion résultante se trouve au voisinage du temps de coupure t_0 pourvu que t_0 se situe avant le maximum de l'impulsion initiale (fig. 6a); si t_0 se situe après le maximum, celui-ci est aussi le maximum de l'impulsion résultante (fig. 6b). D'autre part, pour obtenir un temps de résolution aussi petit que possible, le seuil du discriminateur dans les circuits de coincidences rapides doit être proche du maximum de la "somme" des deux impulsions coincidentes (fig. 5); celui-ci résulte de l'addition non linéaire des deux impulsions au voisinage de leurs maxima respectifs (fig. 5). Il faut donc choisir le temps de coupure t_0 de telle sorte que la variation relative de l'impulsion en ce point $(\sigma/V)_{t=t_0}$ soit aussi petite que possible (cas a de la fig. 6); ou on doit diminuer la variation relative de l'impulsion à son maximum $(\sigma/V)_{t=t'_m}$ (cas b de la fig. 6).

Dans certains circuits de coincidences rapides (réf. [11]) et [12])), on normalise les impulsions dont on étudie les coincidences en les faisant passer dans des discriminateurs rapides, par exemple du type introduit par Moody (réf. [13])); dans ce cas également, une fluctuation dans l'amplitude de l'impulsion introduit une dispersion dans le temps t_1 où l'impulsion coupe le seuil du discriminateur rapide. Les mêmes remarques sont valables si on limite la hauteur de l'impulsion avec une diode (réf. [1])) ou une lampe amplificatrice saturée (réf. [8])), avant l'élément du circuit de coincidences rapides qui réalise l'addition non linéaire. Dans tous les cas, il y a intérêt à diminuer les fluctuations relatives de l'amplitude de l'impulsion. Il s'agit bien de variation relative de l'amplitude car, si elle augmente, la dispersion relative dans le temps augmente aussi comme le montrent les courbes des fig. 2 à 4; comme les temps t_0, t'_m ou t_1 sont plus ou moins fixés par les conditions de l'expérience (choix du cristal, temps de résolution que l'on désire obtenir, type de discriminateur rapide utilisé, capacité C entre l'anode et la masse), la dispersion absolue dans le temps augmente elle aussi avec les fluctuations relatives en amplitude.

La pente à l'origine de l'impulsion est inversement proportionnelle à la capacité C (éq. (4)). Il y a donc avantage à réduire le plus possible C, comme le montrent les courbes a et b de la figure 4: pour les courbes a (en trait plein, épais et fin), $\tau/RC = 1$ et $\overline{Q}_0/C = 1$; les courbes b sont tracées pour une capacité C dix fois plus grande, mais une même résistance R et un même temps de décroissance τ, autrement dit $\tau/RC = 1/10$ et $\overline{Q}_0/C = 1/10$. Les courbes b s'obtiennent donc simplement à partir des courbes $\tau/RC = 1/10$ de la fig. 3, en divisant les ordonnées par 10. On voit donc, sur la fig. 4, que, pour un même seuil du discriminateur, $V = 0.06$ par exemple, les dispersions dans le temps dues aux fluctuations en amplitude sont beaucoup plus importantes pour une capacité C plus grande.

[11]) G. C. Neilson et D. B. James, Rev. Scient. Instr. **26** (1955) 1018.

[12]) P. Macq et J. Vervier, Rev. Scient. Instr. (à paraître).

[13]) N. F. Moody, G. J. Maclusky et M. O. Deighton, Electronic Engineering **24** (1952) 214.

2.2. VARIATIONS RELATIVES DE L'IMPULSION

Nous avons calculé la variation relative de l'impulsion $\sigma(t)/V(t)$ en fonction de t/τ pour différentes valeurs de τ/RC; comme, dans cette expression, $\overline{Q}_0/C$ s'élimine (éq. (1) et (2)), il n'est plus nécessaire de supposer C constant. Les résultats sont représentés à la fig. 7. On voit que, pour diminuer σ/V, il faut augmenter RC, mais qu'on gagne peu à partir de $RC = 10\tau$. D'autre part, il y a avantage, pour τ/RC donné, à se placer près du minimum des courbes de la fig. 7; le temps de coupure t_0 (cas a de la fig. 6), le temps t'_m du maximum de l'impulsion (cas b de la fig. 6) ou le temps t_1 où l'impulsion passe le niveau du discriminateur rapide (cas où on normalise les impulsions) devront être choisis au voisinage de ce minimum. Le temps t'_m du maximum de l'impulsion est marqué par un cercle sur les courbes de la fig. 7; on voit qu'il est toujours proche du minimum.

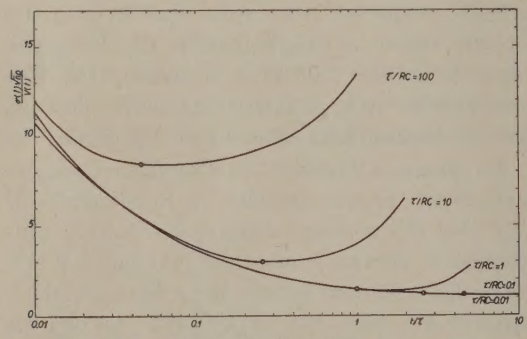

Fig. 7. Variations relatives de l'amplitude des impulsions en fonction de t/τ pour différentes valeurs de τ/RC. Les points marqués par un cercle représentent le maximum des impulsions pour un RC donné.

Etudions quelques cas particuliers: pour obtenir un temps de résolution de 10^{-8} sec par exemple, il faut choisir un temps de coupure t_0 assez petit, de l'ordre de 10^{-8} sec; d'autre part, on a: $C \approx 10\ \mu\mu$F (cf. paragraphe 3). Prenons par exemple le cas de NaI(Tl) ($\tau = 2.5 \times 10^{-7}$ sec): on a $t_0/\tau \approx 0.04$. On voit, sur les courbes de la fig. 7 que, pour cette valeur de t_0/τ, la variation relative ne diminue guère si on passe de $RC = \tau/10$ à $RC = 100\tau$; il faut donc choisir $R \geqslant \tau/10C = 2.5\ \text{k}\Omega$. Pour l'anthracène, $\tau = 3.6 \times 10^{-8}$ sec et $t_0/\tau \simeq 0.3$; dans ce cas, il n'y a pas avantage à augmenter RC au delà de τ. On choisira donc $R \geqslant 3.6\ \text{k}\Omega$. Dans le cas du stilbène, $\tau = 6 \times 10^{-9}$ sec et $t_0/\tau \approx 1.5$; comme pour l'anthracène, il n'est pas nécessaire d'augmenter RC au delà de τ, et il y a avantage à choisir $R \geqslant 600\Omega$. Pour les scintillateurs liquides et plastiques ($\tau \approx 2$ à 3×10^{-9} sec et $t_0/\tau \approx 5$ à 3), la situation est analogue, et la résistance R minimum est de l'ordre de 200 à 300 Ω, c-à-d de l'ordre de grandeur des impédances caractéristiques des lignes de transmission. On notera que pour le stilbène, les scintillateurs liquides et plastiques, on a $t_0/\tau > 1$, et donc le temps de coupure se trouve au delà du maximum de l'impulsion initiale pour $\tau/RC \approx 1$; c'est donc la variation de l'impulsion à ce maximum qui intervient. D'ailleurs, il n'est plus nécessaire, dans ce cas, de couper les impulsions par des cables coaxiaux. Notons enfin que la hauteur des impulsions augmente avec RC; mais on voit, sur les courbes de la fig. 1, que le choix de R préconisé ci-dessus ne diminue que peu l'amplitude de l'impulsion.

Si on compare entre eux les différents cristaux, on remarque sur les courbes de la fig. 7 que, pour le choix de RC préconisé plus haut, les variations relatives en amplitude diminuent si on passe des cristaux lents comme le NaI(Tl) ($t_0/\tau \approx 0.04$) à des cristaux rapides comme le stilbène ($t_0/\tau \approx 1.5$); cela explique la préférence accordée aux cristaux rapides pour des mesures avec temps de résolution très petit.

2.3. VARIATIONS RELATIVES DE L'IMPULSION À SON MAXIMUM

Nous avons calculé la variation relative de l'impulsion à son maximum $(\sigma/V)_{t=t'_m}$ en fonction de τ/RC, d'après les équations (1) à (3); elle représente la meilleure résolution en énergie que l'on peut obtenir avec un cristal et une constante RC donnée. Les résultats sont repris à la fig. 8. On voit que, pour améliorer cette résolution, il faut augmenter RC, mais qu'on gagne peu au delà de $RC \simeq \tau$. Pour des électrons de 1 MeV, détectés par un cristal d'anthracène suivi d'un guide en lucite qui transmet 20% des photons et d'un photomultiplicateur RCA 5819

pour lequel $p \approxeq 5$ à 10%, on peut calculer que $\overline{n}p \approxeq 100$; la meilleure résolution en énergie que l'on peut obtenir est donc de l'ordre de 15%.

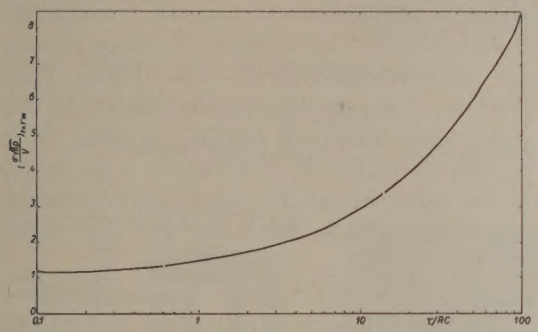

Fig. 8. Variations relatives de l'amplitude de l'impulsion à son maximum en fonction de τ/RC.

2.4. DISPERSION TOTALE DANS LE TEMPS

La dispersion dans le temps Δt_a due aux fluctuations en amplitude de l'impulsion peut se déterminer par la méthode graphique signalée plus haut; elle se combine avec la dispersion Δt_b introduite par le guide de lumière et le photomultiplicateur. La dispersion totale dans le temps, Δt, vaut $\sqrt{\Delta t_a^2 + \Delta t_b^2}$; on l'a représentée graphiquement à la fig. 4, pour $\tau/RC = 1$, $\tau = 6 \times 10^{-9}$ sec et $\Delta t_b = 1.2 \times 10^{-9}$ sec: pour chaque valeur de l'ordonnée (amplitude de l'impulsion), on porte, de part et d'autre de la courbe de l'amplitude (trait plein, épais), la dispersion Δt. On voit que, dans ce cas, Δt_b est du même ordre de grandeur et même plus grand que Δt_a; pour un temps de décroissance τ plus long, Δt_b devient petit devant Δt_a. Il est donc relativement plus important de diminuer les variations en amplitude dans le cas des cristaux lents (NaI) que pour les cristaux rapides (stilbène).

3. Réduction des Dispersions dans le Temps

Comme nous l'avons montré au paragraphe précédent, la capacité parasite C entre l'anode du photomultiplicateur et la masse doit être aussi petite que possible; divers dispositifs expérimentaux se sont révélés avantageux de ce point de vue. Nous avons utilisé, pour notre étude, des photomultiplicateurs RCA 5819; les capacités C, de l'ordre de 10 $\mu\mu$F, ont été mesurées avec un "130 L-C meter, Tektronix".

La capacité C de sortie des phototubes RCA 5819 diminue considérablement si on enlève le culot: elle passe de 6.5 $\mu\mu$F à 3.5 $\mu\mu$F; nous avons donc remplacé le culot par une plaquette en bakélite, support d'un circuit imprimé qui comporte la chaine de résistances des dynodes.

Deux sortes de montages peuvent alors être réalisés suivant le temps de décroissance τ du cristal utilisé. Dans le cas du stilbène et des scintillateurs liquides et plastiques, nous avons montré au paragraphe précédent que la résistance minimum de sortie des photomultiplicateurs, compatible avec une faible dispersion en amplitude, était de l'ordre de grandeur des impédances caractéristiques des lignes de transmission; il n'est donc plus nécessaire, dans ce cas, d'utiliser un cathode-follower pour adapter les impédances: le fil d'anode constitue, dès sa sortie du phototube, le fil central d'un cable coaxial qui conduit directement les impulsions dans les amplificateurs distribués où il est terminé par son impédance caractéristique, 200 Ω .On évite de la sorte, des instabilités possibles dans le cathode-follower; d'autre part, la capacité C se réduira à celle inhérente à la structure interne du tube, C_{int}, le cable coaxial n'y contribuant que fort peu.

Pour les cristaux plus lents que le stilbène, comme l'anthracène et le NaI(Tl), la résistance minimum est plus élevée, et un cathode-follower devient nécessaire; il est réalisé, en circuit imprimé, sur la plaquette de bakélite qui remplace le culot du photomultiplicateur. C se compose alors de C_{int}, de la capacité C_{cabl} due au cablage entre l'anode du phototube et la grille du cathode-follower et de la capacité d'entrée du cathode-follower, C_{in}; dans le cas d'une pentode, on a:

$$C_{in} = C_{gp} + (1 - A)\, C_{gk} \qquad (5)$$

où C_{gp} et C_{gk} sont respectivement les capacités grille-plaque et grille-cathode, et A est le facteur d'amplification du cathode-follower. Le premier terme est petit, si on utilise une pentode; dans le 2°, A est proche de 1 (de l'ordre de 0.8) ce qui diminue l'importance de C_{gk}. On peut inclure, dans C_{gk}, la capacité du cablage C_{cabl} si on

réalise le montage suivant: la connection entre l'anode du photomultiplicateur et la grille du cathode-follower constitue le fil central d'un cable coaxial dont le blindage est relié à la cathode du cathode-follower. De la sorte, la capacité du cablage C_{cabl} et la capacité grille-cathode C_{gk} sont toutes deux réduites du facteur $1 - A \approx 0.2$; les résultats consignés à la table 1 montrent l'intérêt de ce montage. On voit également, d'après la troisième ligne de la table 1, que l'utilisation d'un tube inverseur à la sortie des phototubes augmente C: dans ce cas, A est négatif et l'importance de la capacité C_{gk} est augmentée par le facteur $1 - A$, comme le montre l'équation (5); si le tube inverseur est indispensable, on a intérêt à ne pas inclure C_{cabl} dans C_{gk}, donc à ne pas utiliser de cable coaxial entre l'anode du phototube et la grille du cathode-follower. Notons que l'emploi d'une triode comme cathode-follower ou comme tube inverseur n'est pas à recommander, car la capacité de sortie des photomultiplicateurs serait augmentée dans de fortes proportions par effet Miller.

TABLE 1

	I	II	III
C.F.(1)	10	18.5	13.5
C.F.(2)	10	18.5	8
I	10	18.5	21

Capacité de sortie C, en $\mu\mu$F, des photomultiplicateurs pour différents montages. C.F.(1) représente le montage habituel du cathode-follower avec le blindage du cable coaxial à la masse; pour C.F.(2), le blindage du cable coaxial est relié à la cathode. I est le montage en tube inverseur. Les différentes colonnes donnent les valeurs de C sans tube (I), avec tube éteint (II) et avec tube allumé (III). Le tube est une pentode E 180 F.

4. Conclusion

Pour diminuer les dispersions dans le temps dues aux fluctuations en amplitude des impulsions, on doit réduire la capacité C et choisir convenablement la résistance R entre l'anode des photomultiplicateurs et la masse. Pour diminuer C, il y a avantage à enlever le culot des phototubes; lorsque C est fixé, le choix de R dépend du temps de décroissance τ du cristal utilisé, et du temps t_0 de coupure des impulsions, donc du temps de résolution que l'on désire obtenir.

Dans le cas des cristaux rapides (stilbène, scintillateurs liquides et plastiques), il n'est pas nécessaire d'utiliser un cathode-follower: le cable coaxial part directement de l'anode du photomultiplicateur, et R est la résistance qui termine le cable dans les amplificateurs distribués; pour ces cristaux, la dispersion dans le temps provient surtout du guide de lumière et du photomultiplicateur.

Dans le cas des cristaux plus lents (anthracène, NaI (Tl)...), on utilise un cathode-follower: les impulsions sont conduites de l'anode du photomultiplicateur à la grille du cathode-follower par un cable coaxial dont le blindage est relié à la cathode; la résistance de sortie du phototube doit être choisie suivant le temps de décroissance τ du cristal comme indiqué au paragraphe 2. Pour ces cristaux, la dispersion dans le temps provenant des fluctuations en amplitude est plus importante que celle introduite par le guide de lumière et le photomultiplicateur.

Nous remercions Monsieur le professeur M. de Hemptinne pour ses encouragements au cours de ce travail; nous remercions également M. M. A. Meessen et G. Deutsch pour les précieuses discussions qui ont été à l'origine de cet article et pour leurs critiques bienveillantes et leurs nombreuses suggestions.